TITLE PAGE

Pathological modeling of TBEV infection reveals differential innate immune responses in human neurons and astrocytes that correlate with their susceptibility to infection.

Short title: Pathological modeling and cell-specific TBEV innate immunity

Authors

Mazigh Fares[1,2], Marielle Cochet-Bernoin[1], Gaëlle Gonzalez[1], Claudia N. Montero-Menei[3], Odile Blanchet[4], Alexandra Benchoua[5], Claire Boissart[5], Sylvie Lecollinet[1], Jennifer Richardson[1], Nadia Haddad[6], Muriel Coulpier[1*]

Author affiliation

[1] UMR1161 Virologie, Anses, INRA, Ecole Nationale Vétérinaire d'Alfort, Université Paris-Est, Maisons-Alfort, France

[2]MRC-University of Glasgow Centre for Virus Research, Glasgow, Scotland, United Kingdom

[3] CRCINA, UMR 1232, INSERM, Université de Nantes, Université d'Angers, Angers F-49933, France

[4]CHU Angers, Centre de Ressources Biologiques, BB-0033-00038, Angers, France

[5]CECS, I-STEM, AFM, Evry, France,

[6] UMR BIPAR 956, Anses, INRA, Ecole Nationale Vétérinaire d'Alfort, Université Paris-Est, Maisons-Alfort, France

**Correspondence to:*

Email: muriel.coulpier@vet-alfort.fr

Author contribution

Conceptualization : MF and MC ; Development or design of methodology : MF and MC ; Validation : MF and MC ; Formal analysis : MF ; Investigation : MF, MCB, GG ; Resources : CNMM, OB, AB, CB and SL ; Original draft preparation : MF and MC ; Writing, review and Editing : JR and NH ; Visualization : MF and MC ; Supervision : MC ; Project administration : MC ; Funding acquisition : NH and MC.

Funding information:

This study was financially supported by the French National Institute for Agricultural Research (INRA) and DIM MalInf-Ile de France. MF was financially supported by INRA and the Paris Institute of technology for life, food and environmental sciences (AgroParisTech). GG was funded by Labex IBEID. The funders had no role in study design, data collection and analysis, decision to publish, or preparation of the manuscript.

Number of figures: 9 **Number of tables: 1** **Number of pages: 39**

Number of supplemental figures: 2 **Number of supplemental tables: 1**

Abstract Word Count: 254 **Text Word Count: 6787**

Abstract

Tick-borne encephalitis virus (TBEV) is a member of the *Flaviviridae* family, *Flavivirus* genus, which includes several important human pathogens. It is responsible for neurological symptoms that may cause permanent disability or death, and, from a medical point of view, is the major arbovirus in Central/Northern Europe and North-eastern Asia. TBEV tropism is critical for neuropathogenesis, yet, little is known about the molecular mechanisms that govern the susceptibility of human brain cells to the virus. In this study, we sought to establish and characterize a new *in vitro* model of TBEV infection in the human brain and to decipher cell type-specific innate immunity and its relation to TBEV tropism and neuropathogenesis. We showed that infection of neuronal/glial cultures derived from human fetal neural progenitor cells (hNPCs) mimicked three major hallmarks of TBEV infection in the human brain, namely, preferential neuronal tropism, neuronal death and astrogliosis. We also showed that these cells had conserved their capacity to build an antiviral response against TBEV. TBEV-infected neuronal/glial cells, therefore, represented a highly relevant pathological model. By enriching the cultures in either human neurons or astrocytes, we further demonstrated qualitative and quantitative differential innate immune responses in the two cell types that correlated with their particular susceptibility to TBEV. Our results thus reveal that cell type-specific innate immunity is likely to contribute to shaping TBEV tropism for human brain cells. They offer a new *in vitro* model to further study TBEV-induced neuropathogenesis and improve our understanding of the mechanisms by which neurotropic viruses target and damage human brain cells.

Author summary

Tick-borne encephalitis virus (TBEV), a neurotropic *Flavivirus* that is responsible for encephalitis in humans, is of growing concern in Europe. Indeed, over the last two decades the

number of reported cases has continuously increased and the virus has spread into new geographical areas. Whereas it is well established that neurons are the main target of TBEV in the human brain, the mechanisms that underlie this preferential tropism have not yet been elucidated. Here, we used neuronal/glial cells derived from human fetal neural progenitors to establish and characterize a new *in vitro* pathological model that mimics major hallmarks of TBEV infection *in vivo*; namely, neuronal tropism, neuronal death and astrogliosis. Using this highly relevant model, we showed that human neurons and astrocytes were both capable of developing an innate immune response against TBEV, but with dissimilar magnitudes that correlated with differential susceptibility to TBEV. Our results thus revealed that TBEV tropism for subsets of human brain cells is likely to depend on cell-type specific innate immunity. This improves our understanding of the mechanisms by which neurotropic viruses target and damage human brain cells and may help guide development of future therapies.

Introduction

Tick-borne encephalitis virus (TBEV) belongs to the genus *Flavivirus* (family *Flaviviridae*), whose members include several important human pathogens transmitted by arthropods, such as Japanese encephalitis virus (JEV), West Nile virus (WNV), Zika virus (ZIKV) and Powassan virus (POWV). From a medical point of view, TBEV is the most important arbovirus in Europe and North-eastern Asia. Its endemic zone spreads from Northern, Central and Eastern Europe to Far East Asia (1). It induces a range of symptoms from mild flu-like symptoms to severe encephalitis and paralysis, often with long term neurological sequelae (2). The incidence of the disease has increased in recent decades and autochtonous cases are regularly reported in new areas of Western Europe, reflecting an expansion to non-endemic

97 areas (3). Despite commercialization of an effective vaccine (4), between 8000 and 13000
98 annual cases of tick-borne encephalitis have been reported worldwide since the 1990s (5). No
99 therapy is currently available (6).

100 TBEV is usually transmitted to humans from infected ticks, mainly of the *Ixodes* family,
101 but may occasionally be acquired by consumption of unpasteurized dairy products from
102 infected livestock (7–9). Upon inoculation into the human skin, initial infection and replication
103 occurs in local dendritic cells (DCs). DCs are believed to transport the virus to draining lymph
104 nodes from which it spreads into the bloodstream and induces viremia. It may then cross the
105 blood brain barrier and cause widespread lesions in the brain. These include inflammatory
106 changes, neuronal damage and glial reactivity in several brain areas, including the spinal cord,
107 brainstem, cerebellum and striatum (10,11). Neurons are the primary target of infection (12)
108 but other cells in the CNS may contribute to TBEV-induced neuropathogenesis. Both
109 infiltrating immunocompetent cells, mainly $CD8^+$ T cells, and resident glial cells, such as
110 astrocytes and microglial cells, have been shown to play a role (13,14). Neuronal damage may
111 thus be mediated directly by viral infection or indirectly by infiltrating immunocompetent cells,
112 inflammatory cytokines and activated resident glial cells.

113 The innate immune response is the first line of defense against viral infection. Type I
114 interferons (IFNs) are of particular importance in this process. Through binding to the IFN
115 alpha/beta receptor (IFNAR), they act via autocrine or paracrine signaling (15–17) and trigger
116 the activation of a large number of interferon-stimulated genes (ISGs) that can inhibit almost
117 every step of viral life cycle (18). In recent years, it has become clear that parenchymal cells of
118 the central nervous system (CNS) play a major role in the development of the innate immune
119 response and the protection of infected individuals after CNS infection (19–24). Neurons and
120 astrocytes are not passive targets, as they are known to produce and respond to type I IFNs.

121 Nevertheless, the innate immune programs activated in these cell types during TBEV infection
122 and their impact on viral tropism and neuropathogenesis remain poorly known.

123 Animal models have been widely used to elucidate the cellular and molecular
124 mechanisms of TBEV-induced neuropathogenesis (2). Nevertheless, the results obtained from
125 such studies may be difficult to transpose to human neuropathogenesis, as human anti-viral
126 responses differ substantially from those of other mammalian species (25, 26). The biological
127 relevance of models based on human CNS cells is thus increasingly recognized. These include
128 neuronal/glial cell lines, primary neuronal/glial cells from human fetuses and, more recently,
129 neuronal/glial cells derived from fetal neural progenitors (hNPCs), embryonic (hESC) or
130 induced pluripotent stem cells (hiPSCs). While primary human CNS cells are physiologically
131 more relevant than cell lines, their use is limited by the difficulty in gaining access to cell
132 sources. On the other hand, neuronal/glial cultures derived from neural progenitors are not only
133 physiologically relevant, but also have the advantage of being available on demand. In recent
134 years, they have become important tools to study neurotropic viruses (27).

135 The goal of this study was, first, to set up and characterize a new *in vitro* model of TBEV
136 infection using complex co-cultures of hNPC-derived neuronal/glial cells, and second, to
137 decipher cell-specific anti-TBEV immunity in the human CNS and its relation to TBEV tropism
138 and neuropathogenesis. We showed that *in vitro* TBEV infection mimics several hallmarks of
139 *in vivo* infection, including marked neuronal tropism and neuronal death, limited astrocyte
140 susceptibility, astrogliosis and induction of an antiviral response. Moreover, we demonstrated
141 differential qualitative and quantitative antiviral capacities in human neurons and astrocytes
142 that are correlated with their susceptibility to TBEV infection. Finally, we showed that human
143 astrocytes exert a protective effect on neighboring TBEV-infected neurons.

144

Results

TBEV infects brain cells differentiated from human fetal neural progenitors

HNPCs and their derived neuronal/glial cells were previously set up in our laboratory for the study of Borna disease virus, a neurotropic virus that belongs to the *Bornaviridae* family (28, 29). Here, we used the same hNPCs prepared according to the experimental steps summarized in Fig. 1A. HNPCs were differentiated for 13 days, by which time all neurons were generated (29), before infection with the TBEV-Hypr strain at MOI 10^{-2}. Infected neuronal/glial co-cultures were then analyzed over time. We first examined the capacity of the virus to infect, replicate and disseminate within the co-culture. Examination of cells immunostained with an antibody specific for domain 3 of the TBEV envelope protein (TBEV-E3), at 24 and 72 hours post-infection (hpi), revealed that TBEV entered human brain cells and spread within the co-culture (Fig. 1B). Enumeration of infected cells from 14 hpi to 7 dpi showed that 7.3±0.7% of cells were indeed infected at 14 hpi whereas 45.0±4.0% were infected at 72 hpi, at the peak of infection (Fig. 1C). At a later time, 7 dpi, the number of infected cells decreased. A similar pattern of infection was observed when the viral RNA was quantified by RT-qPCR, whether in the supernatant or intracellularly, from 14 hpi to 7 dpi (Fig. 1D) with an increase in viral RNA observed up to 48-72 hpi followed by a decrease from 96 hpi to 7 dpi. This confirmed active replication of the virus in hNPC-derived brain cells. Quantification of viral titer by end-point dilution further showed that infectious particles were released into the supernatant at 48 and 72 hpi (Fig. 1E). Thus, the infection, replication and dissemination of virus were efficient in hNPC-derived neuronal/glial cells.

TBEV infects human neurons, astrocytes, and oligodendrocytes

We next sought to determine which neural subsets were infected by TBEV in neuronal/glial co-cultures. We had previously shown that, upon growth factor withdrawal, hNPCs differentiated into neurons and astrocytes (28,29). Oligodendrocytes, the third cell type that can be generated by differentiation of hNPCs, were not taken into consideration. To gain in precision, in the present study we enumerated all 3 cell types, based on immunofluorescence staining (S1A Fig), 13 and 21 days after the onset of differentiation. Automatic enumeration of immunostained cells with antibodies directed against HuC/HuD (nuclear markers for neurons) and OLIG2 (nuclear marker for oligodendrocytes) revealed a population composed of 77.0±3.2% (d13) and 74.1±5.4% (d21) neurons and 1.4±1.0% (d13) and 3.7±1.0% (d21) oligodendrocytes (S1B Fig). Due to technical limitations (GFAP localization in astrocytic outgrowths and unavailability of a nuclear marker), astrocytes could not be automatically enumerated. The remaining population, namely total cells minus neurons and oligodendrocytes, comprising 21.5±4.1% (d13) and 22.2±4.4% (d21) of cells, was therefore considered to be composed of astrocytes (S1B Fig). The reliability of this enumeration procedure was confirmed by manual enumeration, as 22.8±5.6% (d13) and 32.7±5.0% (d21) of astrocytes were found using this method (S1C Fig). Thus, we confirmed that neurons and astrocytes were the major cell types in our co-cultures and showed that oligodendrocytes constituted less than 5% of the total cell population.

To characterize TBEV cellular tropism, we infected hNPC-derived neuronal/glial co-cultures and followed infection from 14 hours to 7 days. Cells were co-immunostained with antibodies directed against TBEV-E3 (infected cells) and βIII-tubulin or HuC/HuD (neurons), GFAP (astrocytes) and OLIG2 (oligodendrocytes). At 24 hpi, the 3 cell types were infected, as shown in fig. 2A. Viral envelope strongly accumulated in the perinuclear region of the cytoplasm in all cell types. The protein could also be evidenced in certain neurites and astrocyte

192 outgrowths, albeit with a lower intensity (Fig. 2B). We then sought to determine whether the
193 virus spread within each cellular subpopulation. We therefore quantified infection in each cell
194 type, at different time points during the course of the study (Fig. 2C, 2D, 2E). The general
195 profile of infection was similar in the 3 cell types, with an increase in the first days of infection
196 up until a peak occurring at 48-72 hpi, followed by a decrease at 7 dpi, except for
197 oligodendrocytes in which case no decrease was observed. Early in infection, at 14 hpi, a
198 minority of cells were infected within each subset, namely 7.9±1.2% of neurons, 4.3±1.5% of
199 astrocytes and 11.7±0.8% of oligodendrocytes. Later, however, at the peak of infection, the
200 proportion of infected cells was high in neurons (55.2±3.8%) and oligodendrocytes
201 (68.0±21.5%) but much lower in astrocytes (13.6±5.3%), revealing differential propagation of
202 the virus within the three sub-population. Thus, whereas human neurons and oligodendrocytes
203 were highly susceptible to TBEV infection, human astrocytes were more resistant.
204

205 **TBEV induces death of neurons and astrocytes**

206 As hNPC-derived neuronal/glial cells were highly infected, we then sought to evaluate
207 whether TBEV induced cellular damages. Cultures were infected and cells were fixed at several
208 time points from 14 hpi to 14 dpi before immunostaining with antibodies specific for neuronal
209 and glial cells, as previously described. We first examined the neuronal population. At 14 dpi,
210 examination of HuC/HuD immunostaining revealed that TBEV-infected co-cultures were
211 strongly depleted in neurons, as compared with their non-infected matched controls (Fig. 3A).
212 Enumeration showed that neuronal survival was unaffected in the first days of infection (from
213 14 to 48 hpi), but confirmed that neuronal loss occurred as early as 72 hpi (25.1±5.4% loss) and
214 steadily increased from this point on, reaching 72.0±10.3% at 14 dpi, the latest time point of
215 our study (Fig. 3B). We then examined neuronal morphology based on βIII-tubulin
216 immunostaining. At 7 dpi, a striking loss of neurites was observed in TBEV-infected cultures

as compared with their non-infected matched controls (Fig. 3C). Quantification of total neurite length confirmed their loss not only at 7 dpi (76.1±21.6% decrease), but also at 72 hpi (62.0±22.6% decrease), whereas they were unaffected at an earlier time point (14 hpi) (Fig. 3D). Of note, whereas neuronal death became progressively more pronounced between 72 hpi and 7 dpi, neurite loss peaked as early as 72 hpi, suggesting that neurites alteration precedes neuronal death. Taken together, these results showed that TBEV infection strongly impaired neuronal survival in the co-cultures and, moreover, suggested that neurite alteration preceded neuronal death.

We next evaluated whether glial cells were damaged. Examination of astrocytes immunostained with an antibody directed against GFAP at 7 dpi revealed hypertrophic cells in TBEV-infected cultures, as compared with their non-infected matched controls (Fig. 4A). This change in morphology is reminiscent of astrogliosis, a common feature of stressed astrocytes. Enumeration of GFAP-positive cells was then carried out at 24 hpi, 72 hpi and 7 dpi. Their number was not significantly altered at the earlier time points, 24 hpi and 72 hpi, but a decrease of 20.7±11.1% was observed at 7 dpi compared with non-infected matched controls (Fig. 4B). Thus, TBEV infection diminished survival of not only neurons but also astrocytes, although in a more moderate manner for the latter. By contrast, enumeration of OLIG-2-positive cells did not reveal a significant difference in oligodendrocyte number in TBEV-infected and non-infected cultures (Fig. 4C), showing that despite direct TBEV infection, survival of oligodendrocytes was unaffected. Taken together, our results demonstrated that subsets of hNPC-derived brain cells, that is, neurons, astrocytes and oligodendrocytes, were differentially affected by TBEV infection. In particular, neurons were highly susceptible as regards both infection and mortality, whereas astrocytes were more resistant. Oligodendrocytes were susceptible to infection, but their survival was unaffected.

242 **Human NPC-derived neuronal/glial co-cultures develop a strong antiviral response to**
243 **TBEV infection**

244 When infected with virus, cells initiate an antiviral response that aims at controlling
245 viral replication. In order to determine whether the human neuronal/glial cells used in our study
246 had conserved the capacity to develop such a response upon TBEV infection, we analyzed the
247 differential expression of 84 human genes involved in the antiviral response, using a PCR array
248 approach. Transcripts from hNPC-derived neuronal/glial cells infected with TBEV for 24 h
249 were pooled from biological triplicates and compared with their matched non-infected controls.
250 The studied genes are shown in fig. 5A. After applying an arbitrary cut-off of 3-fold, 25 genes
251 were shown to be significantly modulated in TBEV-infected cells, amongst which 22 genes
252 were up-regulated and 3 were down-regulated (Fig. 5A). The former category included
253 pathogen recognition receptors (PRRs), cytokines, including IFNβ, and ISGs. Overexpression
254 of nine of these genes, 3 PRRs - IFIH1/MDA5 (Fig. 5B), DDX58/RIG-I (Fig. 5C) and TLR3
255 (Fig. 5D), 3 pro-inflammatory cytokines - CXCL10 (Fig. 5E), CCL5/RANTES (Fig. 5F) and
256 CXCL11 (Fig. 5G) - and 3 ISGs - OAS2 (Fig. 5H), MX1 (Fig.5I) and ISG15 (Fig. 5J) - was
257 confirmed using RT-qPCR. IFI6 (Fig. 5K), an additional ISG that was recently shown to protect
258 cells from *Flavivirus* infection (30), was also shown to be overexpressed. For most of these
259 genes, kinetic analyses further revealed that their expression was activated as early as 7 hpi and
260 progressively increased during the course of infection up to 14 dpi, with the exception of pro-
261 inflammatory cytokines whose expression abruptly decreased at 14 dpi (Fig. 5E-G). The latter,
262 however, remained highly overexpressed, as compared with their matched non-infected
263 controls. These data indicated that TBEV-infected hNPC-derived neuronal/glial cells had the
264 capacity to respond to TBEV infection by developing a strong and lasting antiviral response.
265

Differential antiviral response in human neurons and human astrocytes

Neurons and astrocytes are both known to participate in the antiviral response in the CNS (20, 31). As regards oligodendrocytes, little is known so far (32). Our results, showing high susceptibility of neurons but resistance of astrocytes to TBEV infection, led us to hypothesize that differences in their intrinsic capacity for antiviral defense might underlie their differential susceptibility. In order to test this hypothesis and decipher cell autonomous anti-TBEV innate immunity in the human CNS, we sought to obtain cultures enriched in neurons (henceforth called En-N) or astrocytes (henceforth called En-As) and to compare their antiviral response. Oligodendrocytes were not considered further in this study, as their low number in our cultures precluded enrichment. After differentiation of hNPCs for 13 days, neuronal/glial cells were trypsinized and either directly re-seeded (unsorted cultures henceforth called Uns-C) or enriched for neurons (En-N) or astrocytes (En-As). We showed that the splitting procedure did not alter the neuronal/glial co-cultures (Uns-C). Indeed, four days after re-seeding, phase-contrast microscopy of Uns-C revealed typical neuronal (small sized with neurites) and astroglial (larger, flat, with outgrowths) cells (Fig. 6A), as typically observed in non-trypsinized co-cultures (henceforth called Co-C cells). Cell type composition (74.1±4.1% neurons, 20.8±4.9% astrocytes and 5.1±1.2% oligodendrocytes) and basal expression of antiviral genes (analysis of 84 genes of the antiviral response) were unchanged in Uns-C as compared with Co-C cells (Fig. 6B and Fig. 6C, respectively). Enrichment of neurons and astrocytes was confirmed by phase-contrast microscopy (Fig. 6D and 6F, respectively) and cell enumeration, showing that the En-N population was composed of 94.1±0.4% neurons, 3.1±0.4% astrocytes and 2.8±0.2% oligodendrocytes (Fig. 6E) while the En-As population comprised 53.5±2.7% astrocytes, 35.7±2.8% neurons and 10.8±0.5% oligodendrocytes (Fig. 6 G).

We then sought to determine whether distinct antiviral responses occurred in En-As, En-N and Uns-C upon TBEV infection, which would reflect differential antiviral responses in

291 human neurons and astrocytes. Cells were infected for 24 h and the expression of 84 genes of
292 the antiviral response was compared using the same PCR array as previously described. After
293 application of the usual arbitrary cut-off of 3-fold, 20 genes in TBEV-infected Uns-C, 16 genes
294 in TBEV-infected En-N and 21 genes in TBEV-infected En-As were shown to be significantly
295 up-regulated, as compared with their non-infected matched controls (Fig. 7A). Among the set
296 of over-expressed genes, which overlapped with that of non-trypsinized co-cultures, 13 were
297 common to the three cultures (table 1) while others were specific for En-As or En-N cultures
298 (8/21 and 3/16, respectively). Thus, these results showed that the antiviral program activated
299 by TBEV was partially different in human neurons and astrocytes. Of note, for 12/13 of
300 common genes, the magnitude of up-regulation was correlated to the percentage of astrocytes
301 in the cultures. That is, it was much higher in En-As than in En-N and intermediary in Uns-C
302 (Fig. 7A, table 1), showing that human astrocytes were capable of developing a stronger
303 antiviral response to TBEV than human neurons. To validate the PCR array data and to gain
304 further insight into the kinetics of expression of antiviral genes in each cell types, we performed
305 RT-qPCR at 7, 24, and 72 hpi for 3 PRRs — IFIH1 (MDA5) (Fig. 7B), DDX58 (RIG-I) (Fig.
306 7C), and TLR3 (Fig. 7D) —, two ISGs — OAS2 (Fig. 7E) and MX1 (Fig. 7F) —, and one pro-
307 inflammatory cytokine, CXCL10 (Fig. 7G). Because of their well-known anti-flavivirus
308 activity, the ISGs IFI6 (Fig. 7H) and RSAD2 (viperin) (Fig. 7I) were also studied. In
309 confirmation of the PCR array data, all of these genes were significantly more overexpressed
310 in En-As than in En-N, at both 24 and 72 hpi. In addition, at 72 hpi, gene expression in En-N
311 was either maintained (RIG-I, TLR3, OAS2, viperin, CXCL10) or decreased (MDA5, MX1,
312 IFI6) while it was either maintained (MDA5, TLR3, MX1, viperin) or increased (RIG-I, OAS2,
313 CXCL10, IFI6) in En-As, showing that the duration of antiviral responses was shorter in human
314 neurons than astrocytes. The induction of an astrocyte-specific antiviral program, as suggested
315 by the selective overexpression of 8 genes in En-As (Fig. 7A, Table 1), was further confirmed

by the results of RT-qPCR. Not only TLR3 but also viperin were amongst those genes, as upregulation was observed in En-As at 24 hpi and 72 hpi but not in En-N at either time point (Fig. 7D and Fig. 7I). Thus, taken together, these results show that TBEV infection induces an antiviral response in human neurons and astrocytes that is characterized by activation of an overlapping set of genes. This anti-viral program, however, was of greater intensity and longer duration in human astrocytes than in human neurons. The anti-viral programs of the two cell types were also notably distinct, as exemplified by selective overexpression of the gene encoding viperin, well-known for its anti-TBEV activity (33,34), in human astrocytes. In sum, our results revealed a stronger and broader antiviral response in human astrocytes than in human neurons, in keeping with their differential susceptibility to TBEV infection, astrocytes being more resistant and neurons more susceptible.

Table 1

		Fold regulation		
Gene name		**Uns-C**	**En-Ne**	**En-As**
CXCL10		**1024,0**	**415,9**	**1209,3**
MX1		**367,1**	**39,1**	**975,5**
CCL5		**680,3**	**265,0**	**814,6**
IFNB1		**149,1**	**71,5**	**537,5**
OAS2		**215,3**	**23,9**	**498,0**
CXCL11		**270,6**	**126,2**	**388,0**
ISG15		**61,8**	**31,8**	**105,4**
IFIH1		**32,7**	**19,7**	**35,3**
DHX58		**13,2**	**10,6**	**28,2**
CASP1		**10,5**	**6,3**	**24,6**
CXCL8		**28,4**	**11,4**	**23,1**
DDX58		**10,5**	**5,7**	**16,0**
IL6		**7,4**	**10,6**	**8,2**
STAT1		**5,8**	*2,5*	**7,5**

TLR3		**6,2**	*1,7*	**6,4**
IRF7		**5,0**	*0,9*	**5,3**
CTSS		**4,3**	*1,3*	**5,2**
TRIM25		**3,6**	*2,2*	**4,5**
AIM2		*0,9*	*1,0*	**4,0**
MYD88		*2,4*	*1,1*	**3,7**
TNF		**4,5**	*2,6*	**3,7**
IL15		**3,8**	**3,3**	*2,3*
IFNA1		*0,9*	**3,6**	*1,2*
IL12B		*0,9*	**5,9**	*1,2*

Differential expression of antiviral genes in human neurons and astrocytes following TBEV infection may reflect differential baseline expression in the two cell types. To test this hypothesis, non-infected En-N, Uns-C and En-As cells were cultured for 4 days and transcripts from 3 biological samples in each condition were pooled and compared using the human antiviral response PCR array. Antiviral gene expression in En-N was compared with that of Uns-C (Fig. 7J) and En-As (Fig. 7K). Although in both cases, most of the immunity-related genes were not differentially expressed to a significant extent (above the 3-fold threshold recommended by the manufacturer), we observed that the general tendency was to a slight overexpression in astrocytes, since the number of significantly overexpressed genes increased as the percentage of astrocytes increased in the culture, from Uns-C to En-A. Five/84 genes were, indeed, overexpressed in Uns-C compared with En-N (Fig. 6J), while their number rose to 14/84 genes when En-As were compared with En-N (Fig. 6K). By contrast, very few of these genes (3/84) were overexpressed in human neurons, and then only to a modest extent. To validate these results, differential expression of 3 selected genes, 2 PRRs (MDA5 and RIG-I) and 1 ISG (OAS2), was further addressed by RT-qPCR. Significant overexpression of MDA5 (Fig. 7L) and RIG-I (Fig. 7M) in En-As as compared with En-N was confirmed. By contrast, but still in agreement with the PCR array data, no significant difference was observed for the

OAS2 gene (Fig. 7N). These results thus showed that the basal level of expression of certain antiviral genes was higher, albeit slightly, in human astrocytes than in human neurons.

Human astrocytes protected human neurons from TBEV infection and TBEV-induced damage.

Next, we wondered whether human astrocytes might participate in neuronal defense. We reasoned that, if this were the case, neurons would be more sensitive to TBEV infection in cultures depleted of astrocytes. We therefore compared neuronal susceptibility and vulnerability to TBEV infection in Uns-C and En-N, composed of 20.8±4.9% and 3.1±0.4% of astrocytes, respectively. Uns-C and En-N were infected for 24h and the percentage of TBEV-infected neurons within the total neuronal population was quantified based on βIII-tubulin and TBEV-E3 immunostaining. A 30% increase in infected cells was observed in En-N compared with Uns-C (Fig. 8A), showing that, in the absence of astrocytes, neurons were more sensitive to TBEV infection. At that time, neuronal survival was altered neither in TBEV-infected Uns-C nor in TBEV-infected En-N, as revealed by observation of βIII-tubulin immunostaining (Fig. 8B) and enumeration of neurons (S2 Fig.). At 72 hpi, however, a more dramatic alteration of neuronal morphology was observed in TBEV-infected En-N, as compact clusters, characteristic of intense neuronal death, were formed (Fig. 8B). Due to these clusters, it was not possible to enumerate the neurons, but our results clearly showed that, at 72 hpi, neurons were more dramatically affected in cultures deprived of astrocytes. Thus, taken together, these results showed that, upon TBEV infection, the presence of astrocytes was protective for human neurons.

Discussion

Despite its importance in human health, TBEV-induced neuropathogenesis is still poorly understood. So far, most studies have used either *in vitro* or *in vivo* rodent models. Whereas these models have advanced understanding, extrapolation to human neuropathogenesis may not always be relevant, as cellular responses display profound differences between species (25,26, 35). Here we used neuronal/glial cultures derived from human fetal neural progenitor cells as a more accurate *in vitro* model to study anti-TBEV innate immunity and its relation to tropism and neuropathogenesis in the human brain. We developed a new *in vitro* model that mimics major hallmarks of TBEV infection in the human brain, namely, neuronal tropism, neuronal death and astrogliosis, thereby providing a unique and highly relevant pathological model for studying TBEV-induced neuropathogenesis. Moreover, we revealed that a cell-type-specific innate antiviral state in human neurons and astrocytes correlates with their differential susceptibility and vulnerability to TBEV, which strongly suggests that the innate antiviral response shapes TBEV tropism for human brain cells.

Understanding viral tropism is critical for understanding virus-induced neuropathogenesis. Some viruses, like Zika virus, preferentially infect neural progenitors (36,37) whereas human immunodeficiency virus has a strong affinity for microglial cells (38), JC virus for astrocytes (39) and the JHM strain of mouse hepatitis virus (JHMV) for oligodendrocytes (40). Flaviviruses such as TBEV, WNV and JEV have a preferential tropism for neurons, a feature that has been observed in human patients (12,41,42), as well as in rodent models (43,44). Using human neuronal/glial cultures, we reproduced the preferential neuronal tropism that is observed *in vivo* in showing a high percentage of infected neurons (approximately 55% at the peak of infection) together with a low percentage of infected astrocytes (less than 15 %). The limited capacity of the virus to infect astrocytes, as observed in our cultures, as well as in monocultures of rat or human astrocytes (45–47), may explain the

399 lack of detection of infected astrocytes in post-mortem brain tissues from patients with tick-
400 borne encephalitis (12), or their rare detection in Langat virus-infected mice (44), as
401 infrequently infected cells are likely to escape detection. Similar observations have been made
402 for other neurotropic viruses (48–50). Unexpectedly, we also observed infection of
403 oligodendrocytes in the human neuronal/glial cultures, a finding that has never been reported
404 previously. The *in vivo* significance of this observation is at present unknown, especially
405 because the degree of maturation of oligodendrocytes in our culture is undefined, the OLIG2
406 antibody recognizing mature and immature cells indiscriminately (51). However, this should
407 be kept in mind for future examination of brain tissues from infected patients. As these cells
408 represent about 5 % of the total cell population in our cultures, we believe them to have a minor
409 impact *in vitro* and, as we could not enrich them, they were not further considered and we
410 confined our study to neurons and astrocytes. We questioned the reasons that may explain
411 difference in TBEV tropism for these two cell types. This may be due to differential expression
412 of cellular factors that are necessary for establishing a full viral cycle (entry and post-entry
413 events), but the similar percentage of infected neurons and astrocytes that we observed in the
414 first 14 hours following TBEV infection does not lend support for this hypothesis. An
415 alternative hypothesis would be differential capacity of the cell types to develop a protective
416 antiviral response. The innate immune response, a major component of the antiviral response,
417 has indeed been proven to be critically important in restricting infection by neurotropic viruses
418 (52–54) and in determining TBEV tropism in different brain areas in murine models (44,55).
419 Also, studies using rodent models have shown that distinct brain cell types develop different
420 antiviral states. Microglia and astrocytes, for example, which were initially considered to be the
421 sole sentinels that respond to microbial infection within the brain (56,57) have been shown to
422 behave differently, as microglia developed a more robust response than astrocytes to TLR7
423 activation (58). Neurons, long considered to be merely passive targets, are now known to

participate in the antiviral response and viral restriction (19–21,59) and in humans, neurons and astrocytes have been shown to produce and respond to IFNα/β. Despite a general assumption that astrocytes are more important players in antiviral response than neurons, the relative contribution of each cell types has, however, not been formally demonstrated, as direct comparison has never been made, whether in animal or in human *in vitro* models. Here we provided the first evidence that human neurons derived from fetal neural progenitor cells possess all of the necessary machinery to mount a cell-intrinsic antiviral response against TBEV, as they up-regulated IFNβ, ISGs and pro-inflammatory cytokine mRNAs upon TBEV infection. We also demonstrated for the first time that human neurons and astrocytes differ in their capacity to mount an anti-TBEV response. Differences were indeed observed in the repertoire of the antiviral program that is activated in the two cell types upon TBEV infection, with certain genes over-expressed in astrocytes but not in neurons, such as the RSAD2 gene (encoding viperin), an ISG that has been shown to be highly important for controlling TBEV (33,34) and other flaviviruses (55) in the rodent's CNS. Quantitative differences were also observed as transcripts encoding PRRs and genes of IFN signaling were over-expressed with different magnitudes in human neurons and astrocytes, with a stronger and more durable response in astrocytes than in neurons. Our results thus show that the cell-type specific anti-TBEV response is correlated with the susceptibility of human neurons and astrocytes to TBEV, which strongly suggests that innate antiviral response is responsible for shaping TBEV tropism in human brain cells. Whether the high neuronal susceptibility to TBEV infection is due to a weaker general antiviral program in human neurons, involving multiple components of the IFN response, from the PRRs to ISGs, or rather to lower expression of specific ISGs, such as the RSAD2 or IFI6 genes, that are dedicated to the control of flaviviruses (30), remains to be elucidated. It also remains to be determined whether the antiviral response of neurons is weak in response to infection by any neurotropic viruses, or only by certain viruses, such as

449 flaviviruses, or whether it is specific to TBEV infection. Our observation that the baseline
450 expression of certain antiviral genes is lower in neurons than in astrocytes may argue in favor
451 of the first possibility, a hypothesis that should be addressed in future studies. In contrast to our
452 results, TBEV infection in the human neuronal DAOY cells, a human neuroblastoma, led to
453 overexpression of the RSAD2 gene (60), a discrepancy that may be due to the use of non-
454 physiological, immortalized cells in the study from Selinger et al. (2017). Of note, our results
455 showed that neuronal tropism of TBEV does not depend only on the cell-specific antiviral
456 response in human neurons, as the presence of astrocytes in the culture limited their infection
457 and favored their survival. As it was previously reported that murine astrocytes infected with
458 TBEV were protective to neurons through IFN signaling (45), and as we showed that IFNβ was
459 highly up-regulated by human astrocytes upon TBEV infection, we speculate that IFNβ
460 produced by astrocytes acts in a paracrine manner to restrict neuronal infection in our human
461 neuronal/glial co-cultures.

462 Viral tropism and pathogenesis are intimately linked, but how the former governs the
463 latter in the human CNS, during TBEV infection, is incompletely understood. TBEV
464 preferentially infects and kills the neurons (12), a highly dramatic event, as neurons have a very
465 poor capacity to regenerate. Neuronal death may occur either in direct or indirect manners, such
466 as, in the latter case, by inducing secretion of neurotoxic proteins by resident glial cells or
467 recruitment of peripheral inflammatory cells to the brain parenchyma (11,14). Involvement of
468 T cells in neuronal death cannot be explored in our model. However, it has to be noted that
469 chemokines such as CXCL10, CCL5 and CXCL11, which have been shown to be over-
470 expressed in the cerebrospinal fluid of human patients infected with TBEV (61–63), are highly
471 up-regulated by both human neurons and astrocytes, revealing that the two cell types may
472 participate in chemo-attraction of T cells into TBEV-infected human brain parenchyma. Similar
473 to the observation made for PRRs and ISGs, their overexpression was, however, stronger in

474 astrocytes than in neurons, showing that astrocytes may be a major player in this process as
475 well. As for neuronal death due to direct infection by TBEV, it has not yet been demonstrated,
476 although ultrastructural changes in response to TBEV infection have been observed (64,65). In
477 our human neuronal/glial and enriched neuron cultures, neuronal death occurred in the absence
478 of peripheral cells and was associated with infection of a large proportion of neurons, showing
479 that the virus is directly responsible for their death. This is likely to play an important role in
480 the human brain upon infection with TBEV and most probably other flaviviruses, since similar
481 conclusions have been drawn for West Nile virus in studies performed in primary murine
482 neurons (66). Reactive astrocytes, however, may also influence neuronal death. Astrogliosis,
483 indeed, occurs following brain trauma of diverse etiology (67), including infection by TBEV
484 or the related Langat virus infection (12), and may be either beneficial or detrimental to neurons
485 (68). In human neuronal/glial cultures, we have observed that astrocytes were hypertrophic, a
486 classical feature of reactive astrocytes and, when neurons were deprived of astrocytes, they
487 were more sensitive to TBEV infection, showing that astrocytes exerted, under these conditions,
488 a neuroprotective effect, possibly via restriction of neuronal infection as previously discussed.
489 Thus, the intensity of neuronal death depends not only on direct infection of neurons but also
490 on the indirect effect mediated by reactive astrocytes. Proliferation sometimes accompanied
491 astrocyte hypertrophy in astrogliosis. Surprisingly, in our experiments, we observed a decrease
492 in the number of astrocytes by 7 days following infection, which strongly suggested that TBEV
493 induced astrocytic death. This is in apparent contradiction with previous work showing that
494 astrocyte viability was unaffected in rodent and human astrocyte monocultures (46,47). The
495 difference in our results may be due to differential conditions of infection, such as viral strain
496 or infectious dose or to the presence of neurons in our co-cultures, which may lead to astrocyte
497 death by an unknown mechanism. Of note, infection with TBEV is not always correlated to cell
498 death, since as many as 60 % of oligodendrocytes were infected without impact on their

499 viability. Why certain cell types die upon TBEV infection while others do not remains to be
500 understood, as do the molecular pathways that lead to cell death. Interestingly, our findings
501 suggest that neuronal death may result from axonal pathology and retrograde degeneration.
502 Indeed, we showed that loss of neurites preceded the disappearance of neuronal cell bodies, an
503 observation that is in agreement with previous work in which accumulation of viral protein in
504 neuritic extensions and dendritic degeneration due to local replication of TBEV was evidenced
505 in murine neurons (64). The relative contribution of axonal degeneration, which is known to
506 play a pathogenic role in rabies virus infection (69) and in some neurodegenerative diseases
507 (70), to TBEV-induced neuronal death need to be defined in future studies.

508 Until recently, the lack of relevant *in vitro* models virtually precluded meaningful study
509 of viral pathogenesis in the human brain. This obstacle has been overcome by the development
510 of methodologies providing an unlimited source of human neural cell types that can be used for
511 disease modeling. In this study, we set up a new, complex and highly relevant *in vitro* model
512 that mimics the major events of TBEV infection in the human brain. Using this model, we
513 evidenced differential innate immune responses in human neurons and astrocytes that
514 contribute to shaping TBEV tropism and neuro-pathogenesis. Based on our results, we propose
515 a model for interactions between TBEV and human brain cells that is represented in fig 9. Our
516 study thus advances understanding of the mechanisms involved in TBEV-induced damage of
517 the human brain and provides a pathological model that can be used in the future to provide
518 greater knowledge as well as to develop new therapies by screening for antiviral or
519 neuroprotective drugs.
520
521

Material and methods

Ethics statement

Human fetuses were obtained after legal abortion with written informed consent from the patient. The procedure for the procurement and use of human fetal central nervous system tissue was approved and monitored by the "Comité Consultatif de Protection des Personnes dans la Recherche Biomédicale" of Henri Mondor Hospital, France. The cells are declared at the "Centre de Ressources Biologiques" of the University Hospital in Angers BB-0033-00038 with reference numbers at the Research Ministry: declaration N° DC-2011-1467; authorization N° AC-2012-1507.

Culture of human neural progenitor cells

Human neural progenitor cells (hNPCs) were prepared and cultured as previously described in (28,29)

Neuronal and glial differentiation

hNPCs were seeded on matrigel-coated plates at a density of 30 000 cells/cm². Differentiation to a mixed population of neuronal and glial cells was induced 24 h after plating by replacing N2A medium with 1:1 N2A and NBC media (N2A: advanced Dulbecco'smodified Eagel medium-F12 supplemented with 2mM L-glutamine, 0.1mg/ml apotransferrin, 25µg/ml insulin and 6.3ng/ml progesterone. NBC: Neurobasal medium supplemented with 2mM L-glutamine and B27 without vitamin A 1X - Invitrogen, Life Technologies) and withdrawing EGF (TEBU, France) and bFGF (TEBU, France). Differentiation conditions were maintained for 13 days

544 with medium replacement twice a week, prior to infection. Twenty-four-well plates (IBIDI,
545 #82406) were used for fluorescent immunostaining and 6-well plates (Falcon) were used to
546 prepare lysates for RNA analyses.

547

548 **Virus and infection**

549 TBEV Hypr strain was a kind gift from Dr S. Moutailler (Maisons-Alfort, France). The strain
550 was isolated in 1953 from the blood of a 10-year-old child in the Czech Republic and the
551 complete sequence was published in (71). A working stock was generated in VERO cells
552 (VERO-ATCC-CCL81) cultured in MEM medium (ThermoFisher) supplemented with 2%
553 fetal bovine serum (FBS). Titer was estimated by plaque assay on VERO cells. Neuronal/glial
554 cells differentiated for 13 days were infected with the virus (MOI 10^{-2}) for 1h at 37°C. The
555 inoculum was removed and cells were incubated in fresh N2A-NBC medium. Virus titers were
556 estimated by endpoint dilution on VERO cells (TCID50).

557

558 **RNA isolation and qPCR**

559 RNA was isolated from infected and non-infected neuronal/glial co-cultures. Cells were lysed
560 using the *NucleoMag® 96 RNA* kit (Macherey Nagel) and RNA was extracted with a *King*
561 *Fisher Duo* automat (Fisher Scientific) following the manufacturer's instructions. Extraction of
562 viral RNA from supernatants of infected cells was performed using *QIAamp Viral RNA Mini*
563 *Kit* (Qiagen) according to the manufacturer's instructions. One hundred and sixty ng (Fig. 5) or
564 250 ng (Fig. 7) of RNA were used to synthesize cDNA with the *SuperScript™ II Reverse*
565 *Transcriptase* kit (ThermoFisher Scientific). Real-time PCR was performed using 2µl of cDNA
566 and *QuantiTect SYBR green PCR master* (Qiagen) with a LightCycler 96 instrument (Roche

Applied Science), for a total volume of 20µl of reaction mixture. For relative quantification, the -2ΔΔCt method was used (72). The references genes were *GAPDH* or *HPRT1*. Primers pairs are listed in Supplementary table 1.

RT² profiler PCR array

Equal volumes of RNA from biological triplicates were pooled for each condition. Two hundred to 500 ng of RNA were transcribed with the *RT² First Strand Kit* (SA Biosciences, Qiagen). Synthetized cDNA was subjected to a PCR array specific for the human antiviral response (*RT² Profiler PCR array* – PAHS-122Z, SA Biosciences, Qiagen), according to the manufacturer's instructions. Data were normalized using the *HPRT1* house-keeping gene and analyzed with the -2ΔΔCt method for relative quantification. According to the manufacturer's instructions, an arbitrary cut-off of 3 was applied to determine significant differences. The analysis was performed using the Qiagen Data analysis center (http://www.qiagen.com/fr/shop/genes-and-pathways/data-analysis-center-overview-page/).

Immunofluorescence assays and cell enumeration

Neuronal/glial cells were fixed for 20 minutes in 4% paraformaldehyde in PBS (Electron Microscopy Sciences) and standard immunofluorescence was performed using antibodies for HuC/HuD (Thermofisher #A21271), βIII-tubulin (Sigma #T8660), GFAP (Dako #M076101-2 or #Z033429-2), OLIG2 (R&D Systems #AF2418) and TBEV-E3. Cells were blocked for 1h in 3% BSA (Sigma), 0.3% Triton-X-100 (VWR) in PBS 1X and primary antibodies were incubated in 1% BSA, 0.1% Triton-X-100 in PBS 1X overnight at +4°C. Secondary antibodies were Alexa Fluor-488/546-conjugated anti-mouse/anti-rabbit IgG (Molecular Probes,

590 Invitrogen). Nuclei were stained with 4′, 6-diamidino-2-phenylindole (DAPI) (Life
591 Technologies) at 0.1 ng/ml. Cell sub-types and infected cells were enumerated either manually
592 or automatically. For manual cell quantification (cells immunostained with antibodies directed
593 against βIII-tubulin and GFAP), images were acquired with an *AxioObserver Z1* (Zeiss)
594 inverted microscope using ZEN software (Zeiss) and analyzed using ImageJ 1.49m software.
595 For automated quantification (cells immunostained with antibodies directed against HuC/HuD,
596 TBEV-E3 and OLIG2 or neurites immunostained with an antibody against βIII-tubulin), images
597 were acquired using the Cellomics ArrayScan automated microscope (Thermofisher Scientific)
598 and analyzed using "Colocalization" or "Neuronal profiling" bio-applications on HCS Studio
599 Cell Analysis Software V6.6.0 (Thermofisher Scientific). In all experiments, an average of 1200
600 (manual quantification) or 5000 (automated quantification) cells per well were enumerated. The
601 digitized images shown were adjusted for brightness and contrast using ImageJ, without further
602 alteration.

603

604 **Magnetic-activated cell sorting**

605 Neuronal/glial cells differentiated for 13 days were detached using Gibco™ TrypLE™ Select
606 Enzyme (1X) and collected into N2A-NBC medium. After centrifugation at 80g for 10 minutes,
607 cells were either sub-cultured (Uns-C) or supplemented with kynurenic acid buffer and sorted
608 according the manufacturer's instructions using the Microbead Kit (Miltenyi Biotec #130-095-
609 826). In brief, resuspended cells were incubated 10 minutes at 4°C with 20µl biotin-conjugated
610 anti-GLAST (ACSA-1) antibodies per 10^7 cells, washed and incubated with anti-biotin
611 MicroBeads for 15 minutes at 4°C. Cell sorting was performed using MS columns (Miltenyi
612 Biotec, #130-042-201) placed in a MiniMACS^{TM} separator (Miltenyi Biotec #130-090-312).
613 The cell fractions found in the flow-through or bound to beads were composed of enriched

614 neurons (En-N) and enriched astrocytes (En-As), respectively. Both sorted and unsorted cells
615 were seeded at a density of 100 000 cells per cm² on 24-well µ-plates (IBIDI, #82406) in N2A-
616 NBC or conditioned medium (1:1, fresh N2A-NBC: supernatant of non-infected co-cultures
617 differentiated for 13 days, conditioned for 48h). Conditioned medium allowed neuronal survival
618 in En-N cultures. Half of the medium was replaced every other day.

619

620 **Statistical analyses**

621 Data are represented as mean ± standard deviation (SD). Statistical analyses were performed
622 with GraphPad Prism V4.03 or V6.0.1 using an unpaired Student's t test or a one-way ANOVA
623 analysis (Bonferroni's Multiple Comparison Test), *=($p<0,05$), **=($p<0,01$), ***=($p<0,001$),
624 non-significant (ns)= ($p>0,05$).

625

626

627 ## Acknowledgments

628 We are most grateful to Dr S Moutailler for providing the TBEV-Hypr strain. We deeply thank
629 Drs PE Ceccaldi and T Couderc for sharing their insight and Dr N Jouvenet for critical reading
630 of the manuscript.

631

632 ## References

633 1. Dumpis U, Crook D, Oksi J. Tick-borne encephalitis. Clin Infect Dis Off Publ Infect Dis Soc Am. avr
634 1999;28(4):882‑90.

2. Růžek D, Dobler G, Donoso Mantke O. Tick-borne encephalitis: pathogenesis and clinical implications. Travel Med Infect Dis. juill 2010;8(4):223‑32.

3. Caracciolo I, Bassetti M, Paladini G, Luzzati R, Santon D, Merelli M, et al. Persistent viremia and urine shedding of tick-borne encephalitis virus in an infected immunosuppressed patient from a new epidemic cluster in North-Eastern Italy. J Clin Virol Off Publ Pan Am Soc Clin Virol. août 2015;69:48‑51.

4. Heinz FX, Holzmann H, Essl A, Kundi M. Field effectiveness of vaccination against tick-borne encephalitis. Vaccine. 23 oct 2007;25(43):7559‑67.

5. Donoso Mantke O, Escadafal C, Niedrig M, Pfeffer M, Working Group For Tick-Borne Encephalitis Virus C. Tick-borne encephalitis in Europe, 2007 to 2009. Euro Surveill Bull Eur Sur Mal Transm Eur Commun Dis Bull. 29 sept 2011;16(39).

6. Ruzek D, Avšič Županc T, Borde J, Chrdle A, Eyer L, Karganova G, et al. Tick-borne encephalitis in Europe and Russia: Review of pathogenesis, clinical features, therapy, and vaccines. Antiviral Res. avr 2019;164:23‑51.

7. Balogh Z, Ferenczi E, Szeles K, Stefanoff P, Gut W, Szomor KN, et al. Tick-borne encephalitis outbreak in Hungary due to consumption of raw goat milk. J Virol Methods. févr 2010;163(2):481‑5.

8. Brockmann SO, Oehme R, Buckenmaier T, Beer M, Jeffery-Smith A, Spannenkrebs M, et al. A cluster of two human cases of tick-borne encephalitis (TBE) transmitted by unpasteurised goat milk and cheese in Germany, May 2016. Euro Surveill Bull Eur Sur Mal Transm Eur Commun Dis Bull. avr 2018;23(15).

9. Dorko E, Hockicko J, Rimárová K, Bušová A, Popaďák P, Popaďáková J, et al. Milk outbreaks of tick-borne encephalitis in Slovakia, 2012-2016. Cent Eur J Public Health. déc 2018;26 Suppl:S47‑50.

10. Růžek D, Salát J, Singh SK, Kopecký J. Breakdown of the blood-brain barrier during tick-borne encephalitis in mice is not dependent on CD8+ T-cells. PloS One. 2011;6(5):e20472.

11. Gelpi E, Preusser M, Laggner U, Garzuly F, Holzmann H, Heinz FX, et al. Inflammatory response in human tick-borne encephalitis: analysis of postmortem brain tissue. J Neurovirol. août 2006;12(4):322‑7.

12. Gelpi E, Preusser M, Garzuly F, Holzmann H, Heinz FX, Budka H. Visualization of Central European tick-borne encephalitis infection in fatal human cases. J Neuropathol Exp Neurol. juin 2005;64(6):506‑12.

13. Hayasaka D, Nagata N, Fujii Y, Hasegawa H, Sata T, Suzuki R, et al. Mortality following peripheral infection with tick-borne encephalitis virus results from a combination of central nervous system pathology, systemic inflammatory and stress responses. Virology. 20 juill 2009;390(1):139‑50.

14. Růzek D, Salát J, Palus M, Gritsun TS, Gould EA, Dyková I, et al. CD8+ T-cells mediate immunopathology in tick-borne encephalitis. Virology. 5 févr 2009;384(1):1‑6.

15. Lazear HM, Pinto AK, Vogt MR, Gale M, Diamond MS. Beta interferon controls West Nile virus infection and pathogenesis in mice. J Virol. juill 2011;85(14):7186‑94.

16. Stetson DB, Medzhitov R. Antiviral defense: interferons and beyond. J Exp Med. 7 août 2006;203(8):1837‑41.

17. Takeuchi O, Akira S. Innate immunity to virus infection. Immunol Rev. janv 2009;227(1):75‑86.

18. González-Navajas JM, Lee J, David M, Raz E. Immunomodulatory functions of type I interferons. Nat Rev Immunol. 6 janv 2012;12(2):125‑35.

19. Cho H, Proll SC, Szretter KJ, Katze MG, Gale M, Diamond MS. Differential innate immune response programs in neuronal subtypes determine susceptibility to infection in the brain by positive-stranded RNA viruses. Nat Med. avr 2013;19(4):458‑64.

20. Delhaye S, Paul S, Blakqori G, Minet M, Weber F, Staeheli P, et al. Neurons produce type I interferon during viral encephalitis. Proc Natl Acad Sci U S A. 16 mai 2006;103(20):7835‑40.

21. Detje CN, Lienenklaus S, Chhatbar C, Spanier J, Prajeeth CK, Soldner C, et al. Upon intranasal vesicular stomatitis virus infection, astrocytes in the olfactory bulb are important interferon Beta producers that protect from lethal encephalitis. J Virol. mars 2015;89(5):2731‑8.

22. Hou Y-J, Banerjee R, Thomas B, Nathan C, García-Sastre A, Ding A, et al. SARM is required for neuronal injury and cytokine production in response to central nervous system viral infection. J Immunol Baltim Md 1950. 15 juill 2013;191(2):875‑83.

23. Schultz KLW, Vernon PS, Griffin DE. Differentiation of neurons restricts Arbovirus replication and increases expression of the alpha isoform of IRF-7. J Virol. janv 2015;89(1):48‑60.

24. Weber E, Finsterbusch K, Lindquist R, Nair S, Lienenklaus S, Gekara NO, et al. Type I interferon protects mice from fatal neurotropic infection with Langat virus by systemic and local antiviral responses. J Virol. nov 2014;88(21):12202‑12.

25. Mestas J, Hughes CCW. Of mice and not men: differences between mouse and human immunology. J Immunol Baltim Md 1950. 1 mars 2004;172(5):2731‑8.

26. Shaw AE, Hughes J, Gu Q, Behdenna A, Singer JB, Dennis T, et al. Fundamental properties of the mammalian innate immune system revealed by multispecies comparison of type I interferon responses. PLoS Biol. 2017;15(12):e2004086.

27. Lafaille FG, Ciancanelli MJ, Studer L, Smith G, Notarangelo L, Casanova J-L, et al. Deciphering Human Cell-Autonomous Anti-HSV-1 Immunity in the Central Nervous System. Front Immunol. 2015;6:208.

28. Brnic D, Stevanovic V, Cochet M, Agier C, Richardson J, Montero-Menei CN, et al. Borna disease virus infects human neural progenitor cells and impairs neurogenesis. J Virol. mars 2012;86(5):2512‑22.

29. Scordel C, Huttin A, Cochet-Bernoin M, Szelechowski M, Poulet A, Richardson J, et al. Borna disease virus phosphoprotein impairs the developmental program controlling neurogenesis and reduces human GABAergic neurogenesis. PLoS Pathog. avr 2015;11(4):e1004859.

30. Richardson RB, Ohlson MB, Eitson JL, Kumar A, McDougal MB, Boys IN, et al. A CRISPR screen identifies IFI6 as an ER-resident interferon effector that blocks flavivirus replication. Nat Microbiol. 2018;3(11):1214‑23.

31. Farina C, Aloisi F, Meinl E. Astrocytes are active players in cerebral innate immunity. Trends Immunol. mars 2007;28(3):138‑45.

32. Bsibsi M, Ravid R, Gveric D, van Noort JM. Broad expression of Toll-like receptors in the human central nervous system. J Neuropathol Exp Neurol. nov 2002;61(11):1013‑21.

713 33. Panayiotou C, Lindqvist R, Kurhade C, Vonderstein K, Pasto J, Edlund K, et al. Viperin Restricts Zika
714 Virus and Tick-Borne Encephalitis Virus Replication by Targeting NS3 for Proteasomal Degradation. J
715 Virol. 01 2018;92(7).

716 34. Upadhyay AS, Vonderstein K, Pichlmair A, Stehling O, Bennett KL, Dobler G, et al. Viperin is an iron-
717 sulfur protein that inhibits genome synthesis of tick-borne encephalitis virus via radical SAM domain
718 activity. Cell Microbiol. juin 2014;16(6):834‑48.

719 35. Lin C-C, Wu Y-J, Heimrich B, Schwemmle M. Absence of a robust innate immune response in rat
720 neurons facilitates persistent infection of Borna disease virus in neuronal tissue. Cell Mol Life Sci
721 CMLS. nov 2013;70(22):4399‑410.

722 36. Ferraris P, Cochet M, Hamel R, Gladwyn-Ng I, Alfano C, Diop F, et al. Zika virus differentially infects
723 human neural progenitor cells according to their state of differentiation and dysregulates
724 neurogenesis through the Notch pathway. Emerg Microbes Infect. 2019;8(1):1003‑16.

725 37. Retallack H, Di Lullo E, Arias C, Knopp KA, Laurie MT, Sandoval-Espinosa C, et al. Zika virus cell
726 tropism in the developing human brain and inhibition by azithromycin. Proc Natl Acad Sci U S A. 13
727 2016;113(50):14408‑13.

728 38. Cosenza MA, Zhao M-L, Si Q, Lee SC. Human brain parenchymal microglia express CD14 and CD45
729 and are productively infected by HIV-1 in HIV-1 encephalitis. Brain Pathol Zurich Switz. oct
730 2002;12(4):442‑55.

731 39. Aksamit AJ, Sever JL, Major EO. Progressive multifocal leukoencephalopathy: JC virus detection by in
732 situ hybridization compared with immunohistochemistry. Neurology. avr 1986;36(4):499‑504.

733 40. Kapil P, Butchi NB, Stohlman SA, Bergmann CC. Oligodendroglia are limited in type I interferon
734 induction and responsiveness in vivo. Glia. oct 2012;60(10):1555‑66.

735 41. Guarner J, Shieh W-J, Hunter S, Paddock CD, Morken T, Campbell GL, et al. Clinicopathologic study
736 and laboratory diagnosis of 23 cases with West Nile virus encephalomyelitis. Hum Pathol. août
737 2004;35(8):983‑90.

738 42. Iwasaki Y, Zhao JX, Yamamoto T, Konno H. Immunohistochemical demonstration of viral antigens in
739 Japanese encephalitis. Acta Neuropathol (Berl). 1986;70(1):79‑81.

740 43. Kimura-Kuroda J, Ichikawa M, Ogata A, Nagashima K, Yasui K. Specific tropism of Japanese
741 encephalitis virus for developing neurons in primary rat brain culture. Arch Virol. 1993;130(3‑4):477
742 ‑84.

743 44. Kurhade C, Zegenhagen L, Weber E, Nair S, Michaelsen-Preusse K, Spanier J, et al. Type I Interferon
744 response in olfactory bulb, the site of tick-borne flavivirus accumulation, is primarily regulated by
745 IPS-1. J Neuroinflammation. 27 janv 2016;13:22.

746 45. Lindqvist R, Mundt F, Gilthorpe JD, Wölfel S, Gekara NO, Kröger A, et al. Fast type I interferon
747 response protects astrocytes from flavivirus infection and virus-induced cytopathic effects. J
748 Neuroinflammation. 24 2016;13(1):277.

749 46. Palus M, Bílý T, Elsterová J, Langhansová H, Salát J, Vancová M, et al. Infection and injury of human
750 astrocytes by tick-borne encephalitis virus. J Gen Virol. nov 2014;95(Pt 11):2411‑26.

751 47. Potokar M, Korva M, Jorgačevski J, Avšič-Županc T, Zorec R. Tick-borne encephalitis virus infects rat
752 astrocytes but does not affect their viability. PloS One. 2014;9(1):e86219.

753 48. Desai A, Shankar SK, Ravi V, Chandramuki A, Gourie-Devi M. Japanese encephalitis virus antigen in
754 the human brain and its topographic distribution. Acta Neuropathol (Berl). 1995;89(4):368‑73.

755 49. German AC, Myint KSA, Mai NTH, Pomeroy I, Phu NH, Tzartos J, et al. A preliminary
756 neuropathological study of Japanese encephalitis in humans and a mouse model. Trans R Soc Trop
757 Med Hyg. déc 2006;100(12):1135‑45.

758 50. Sips GJ, Wilschut J, Smit JM. Neuroinvasive flavivirus infections. Rev Med Virol. mars 2012;22(2):69‑
759 87.

760 51. Yokoo H, Nobusawa S, Takebayashi H, Ikenaka K, Isoda K, Kamiya M, et al. Anti-human Olig2
761 antibody as a useful immunohistochemical marker of normal oligodendrocytes and gliomas. Am J
762 Pathol. mai 2004;164(5):1717‑25.

763 52. Durrant DM, Ghosh S, Klein RS. The Olfactory Bulb: An Immunosensory Effector Organ during
764 Neurotropic Viral Infections. ACS Chem Neurosci. 20 avr 2016;7(4):464‑9.

765 53. Lucas-Hourani M, Munier-Lehmann H, Helynck O, Komarova A, Desprès P, Tangy F, et al. High-
766 throughput screening for broad-spectrum chemical inhibitors of RNA viruses. J Vis Exp JoVE.
767 2014;(87).

768 54. Welsch JC, Charvet B, Dussurgey S, Allatif O, Aurine N, Horvat B, et al. Type I Interferon Receptor
769 Signaling Drives Selective Permissiveness of Astrocytes and Microglia to Measles Virus during Brain
770 Infection. J Virol. 1 juill 2019;93(13).

771 55. Lindqvist R, Överby AK. The Role of Viperin in Antiflavivirus Responses. DNA Cell Biol. sept
772 2018;37(9):725‑30.

773 56. Dong Y, Benveniste EN. Immune function of astrocytes. Glia. nov 2001;36(2):180‑90.

774 57. Hanisch U-K. Microglia as a source and target of cytokines. Glia. nov 2002;40(2):140‑55.

775 58. Madeddu S, Woods TA, Mukherjee P, Sturdevant D, Butchi NB, Peterson KE. Identification of Glial
776 Activation Markers by Comparison of Transcriptome Changes between Astrocytes and Microglia
777 following Innate Immune Stimulation. PloS One. 2015;10(7):e0127336.

778 59. Chakraborty S, Nazmi A, Dutta K, Basu A. Neurons under viral attack: victims or warriors?
779 Neurochem Int. juin 2010;56(6‑7):727‑35.

780 60. Selinger M, Wilkie GS, Tong L, Gu Q, Schnettler E, Grubhoffer L, et al. Analysis of tick-borne
781 encephalitis virus-induced host responses in human cells of neuronal origin and interferon-
782 mediated protection. J Gen Virol. août 2017;98(8):2043‑60.

783 61. Grygorczuk S, Zajkowska J, Swierzbińska R, Pancewicz S, Kondrusik M, Hermanowska-Szpakowicz T.
784 [Concentration of the beta-chemokine CCL5 (RANTES) in cerebrospinal fluid in patients with tick-
785 borne encephalitis]. Neurol Neurochir Pol. avr 2006;40(2):106‑11.

786 62. Lepej SZ, Misić-Majerus L, Jeren T, Rode OD, Remenar A, Sporec V, et al. Chemokines CXCL10 and
787 CXCL11 in the cerebrospinal fluid of patients with tick-borne encephalitis. Acta Neurol Scand. févr
788 2007;115(2):109‑14.

789 63. Zajkowska J, Moniuszko-Malinowska A, Pancewicz SA, Muszyńska-Mazur A, Kondrusik M,
790 Grygorczuk S, et al. Evaluation of CXCL10, CXCL11, CXCL12 and CXCL13 chemokines in serum and
791 cerebrospinal fluid in patients with tick borne encephalitis (TBE). Adv Med Sci. 2011;56(2):311‑7.

64. Hirano M, Yoshii K, Sakai M, Hasebe R, Ichii O, Kariwa H. Tick-borne flaviviruses alter membrane structure and replicate in dendrites of primary mouse neuronal cultures. J Gen Virol. avr 2014;95(Pt 4):849‑61.

65. Bílý T, Palus M, Eyer L, Elsterová J, Vancová M, Růžek D. Electron Tomography Analysis of Tick-Borne Encephalitis Virus Infection in Human Neurons. Sci Rep. 15 juin 2015;5:10745.

66. Shrestha B, Gottlieb D, Diamond MS. Infection and injury of neurons by West Nile encephalitis virus. J Virol. déc 2003;77(24):13203‑13.

67. Liddelow SA, Barres BA. Reactive Astrocytes: Production, Function, and Therapeutic Potential. Immunity. 20 2017;46(6):957‑67.

68. Soung A, Klein RS. Viral Encephalitis and Neurologic Diseases: Focus on Astrocytes. Trends Mol Med. 2018;24(11):950‑62.

69. Li X-Q, Sarmento L, Fu ZF. Degeneration of neuronal processes after infection with pathogenic, but not attenuated, rabies viruses. J Virol. août 2005;79(15):10063‑8.

70. Li J-Y, Conforti L. Axonopathy in Huntington's disease. Exp Neurol. août 2013;246:62‑71.

71. Wallner G, Mandl CW, Ecker M, Holzmann H, Stiasny K, Kunz C, et al. Characterization and complete genome sequences of high- and low- virulence variants of tick-borne encephalitis virus. J Gen Virol. mai 1996;77 (Pt 5):1035‑42.

72. Livak KJ, Schmittgen TD. Analysis of Relative Gene Expression Data Using Real-Time Quantitative PCR and the 2−ΔΔCT Method. Methods. déc 2001;25(4):402‑8.

Legends

Figure 1. TBEV infects, replicates and spreads in hNPC-derived brain cells

(A) Schematic representation of the experimental procedure. (B) Immunofluorescence labeling of differentiated hNPCs 24 h and 72 h following TBEV infection. An antibody directed against the domain 3 of the viral envelope (TBEV-E3, green) revealed infected cells. Nuclei were stained with DAPI (blue). (C) Enumeration of infected cells based on immunofluorescence labeling using an ArrayScan Cellomics instrument. (D) RNA from the supernatant and cell lysate of infected cells was analyzed by RT-qPCR to determine viral replication. (E) Supernatant was collected at the peak of infection and titrated by end-point dilution (TCID50)

822 on VERO cells. Results are representative of 3 independent experiments performed in
823 triplicate. Data are expressed as the mean ± SD. Statistical analysis was performed using one-
824 way ANOVA (Bonferroni's Multiple Comparison Test) with Graphpad Prism V6.0.1, ns=non-
825 significant ($p>0.05$); **=$p<0.01$, ***=$p<0.001$. Scale bar=100µm.

826

827 **Figure 2. TBEV tropism for hNPCs-derived brain cells**

828 HNPCs differentiated for 13 days were infected with TBEV-Hypr at MOI 10^{-2}. (A)
829 Immunofluorescence labeling of infected cells at 24 hpi. Antibodies against βIII-tubulin
830 (neurones), GFAP (astrocytes) or OLIG2 (oligodendrocytes) (green), and TBEV-E3 (red) were
831 used. Nuclei were stained with DAPI (blue). Yellow arrows show infected neurons, astrocytes
832 and oligodendrocytes. Oligodendrocytes were recolored from grey to green. Scale bar=20 µm.
833 (B) Higher magnification (digitally cropped) showing the viral envelope in perinuclear areas
834 (arrowhead) and neurites and astrocytic outgrowths (arrows). Scale bar=20µm. (C-E)
835 Percentage of infected cells based on immunofluorescence labeling during the course of
836 infection for (C) neurons, (D) astrocytes and (E) oligodendrocytes. Results are representative
837 of at least 2 independent experiments performed in triplicate. Data are expressed as the
838 mean±SD. Statistical analysis was performed using a two-tailed unpaired t test with Graphpad
839 Prism V6.0.1, ns=non-significant ($p>0.05$), *=$p<0.05$, **=$p<0.01$, ***=$p<0.001$.

840

841 **Figure 3. TBEV damages human neurons**

842 HNPCs were differentiated for 13 days and infected with TBEV-Hypr at MOI 10^{-2}. (A) Cells
843 in non-infected (NI) and infected (TBEV) co-cultures were immunostained with an antibody
844 directed against HuC/HuD (neurons, green) at 14 dpi. Nuclei were counterstained with DAPI.
845 Scale bars=100µm. (B) Enumeration of HuC/HuD-positive cells using an ArrayScan Cellomics
846 instrument. Normalization to non-infected HuC/HuD-positive cells at 14 hpi. (C) Cells in non-

847 infected and infected cultures were immunostained with an antibody against βIII-tubulin
848 (neurons, red) at 7 dpi. Note the paucity of neurites in TBEV-infected co-cultures. (D)
849 Quantification of neurite network density (neurite length per mm²) using an ArrayScan
850 Cellomics instrument. Results in (B) and (D) are expressed as the mean±SD and are
851 representative of four and two independent experiments performed in triplicate, respectively.
852 Statistical analysis was performed using a two-tailed unpaired t test with Graphpad Prism
853 V6.0.1, ns=non-significant ($p>0.05$); *=$p<0.05$; **=$p<0.01$; ***=$p<0.001$.

854

855 **Figure 4. Impact of TBEV on human glial cells**

856 HNPCs were differentiated for 13 days and infected with TBEV-Hypr at MOI 10^{-2}. (A) Cells
857 in non-infected (NI) and infected (TBEV) co-cultures were immunostained with an antibody
858 directed against GFAP (astrocytes, red) at 7 dpi. Nuclei were counterstained with DAPI. Scale
859 bars=20µm. (B) Manual enumeration of GFAP-positive cells using ImageJ software.
860 Normalization was performed relative to non-infected GFAP-positive cells at 24 hpi. (C)
861 Immunostained cells with OLIG2 antibody were enumerated automatically. Normalization was
862 performed relative to non-infected OLIG2-positive cells at 24 hpi. The results are expressed as
863 the mean±SD and are representative of two (oligodendrocytes) and three (astrocytes)
864 independent experiments performed in triplicate. Statistical analysis was performed using a
865 two-tailed unpaired t test with Graphpad Prism V6.0.1, ns=non-significant ($p>0.05$); *=$p<0.05$.

866

867 **Figure 5. TBEV-induced antiviral response in hNPC-derived neuronal/glial cells**

868 (A) TBEV-infected neuronal/glial cells and their matched NI controls were analyzed 24 hpi using
869 an RT² Profiler PCR array specific for the human antiviral response. The heat map shows the
870 differential expression of 84 analyzed human genes. The most highly up- and down-regulated genes

are colored in red and dark green, respectively. The blue lines indicate the arbitrary cut-off of 3. Genes between the two lines are considered non-regulated. (B-K) RT-qPCR analyses of selected antiviral genes. Gene expression was normalized to *HPRT1* gene and the -2ΔΔCt method was used for relative quantification (normalization to non-infected cells at 7 hpi). Data are expressed as the mean±SD. Results are representative of one experiment performed on pooled triplicates (PCR array) or two independent experiments performed in triplicate (qPCRs). Statistical analysis was performed using a two-tailed unpaired t test with Graphpad Prism V6.0.1, ns=non-significant ($p>0.05$); *=$p<0.05$; **=$p<0.01$; ***=$p<0.001$.

Figure 6. Enrichment of human neurons and astrocytes by magnetic-activated cell sorting

HNPC-derived neuronal/glial cells differentiated for 13 days were sorted using MACS technology. (A, D, F) Phase-contrast micrographs, showing Uns-C (A), En-N (D) and En-As (F), were acquired 96 h after re-seeding. Blue arrows indicate neurons and brown arrowheads indicate astrocytes. Scale bars = 50µm. (B, E, G). Enumeration of neurons, astrocytes and oligodendrocytes in Uns-C (B), En-N (E) and En-As (G) based on immunofluorescence staining (DAPI, antibodies against HuC/HuD and OLIG2) and using an ArrayScan Cellomics instrument. Data are representative of 4 independent experiments performed in triplicate. (C) Scatterplot of basal level of antiviral response genes in unsorted cells (Uns-C) compared with non-trypsinised cells (Co-C). Analysis was performed using an antiviral response PCR array. Genes along the black line have similar expression levels in the two cultures. Dotted lines represent an arbitrary cutoff of 3. Data are from a single experiment performed with pooled triplicates.

Figure 7. Antiviral response in enriched neurons, enriched astrocytes and unsorted cells

(A-I) Expression of antiviral genes upon TBEV infection. (A) TBEV-infected Uns-C, En-N and En-As and their matched non-infected controls were analyzed 24 hpi using an RT^2 profiler PCR array specific for the human antiviral response. Heat map showing the 84 human genes analyzed and their differential expression. Color code and blue line are as in figure 5. Note that genes noted (+) are above the cut-off of 3. (B-I) RT-qPCR analyses of selected antiviral response genes in En-As (red) and En-N (green). (J-N) Basal expression of antiviral genes. (J, K) Scatterplots of basal expression levels of antiviral response genes in enriched neurons (En-N) compared with that of unsorted cells (Uns-C) (J) or enriched astrocytes (En-As) (K). Analysis was performed using an antiviral response PCR array. (L-N) RT-qPCR analysis of the basal expression of IFIH1/MDA5 (L), DDX58/RIG-I (M), and OAS2 (N) genes in En-N and En-As. Gene expression was normalized to HPRT1 and the $-2\Delta\Delta Ct$ method was used for relative quantification (normalization to non-infected En-N, at 7hpi for B-I). The results are expressed as the mean±SD. Data are representative of two independent experiments performed in triplicate (B-I, L-N) and one experiment performed with pooled triplicates (J, K). Statistical analyses comparing En-As and En-N were performed with Graphpad Prism V6.0.1 using a two-tailed unpaired t test, ns=non-significant ($p>0.05$); *=$p<0.05$; **=$p<0.01$; ***=$p<0.001$.

Figure 8 – Human astrocytes protect neurons from TBEV infection

Unsorted cells (Uns-C) and enriched neurons (En-N) were infected with TBEV and co-immunostained using anti-βIII-tubulin and anti-TBEV-E3 antibodies. (A) Infected neurons among the neuronal population. Manual enumeration. The data is displayed as relative infection to Uns-C at 24 hpi. Data are expressed as the mean±SD. (B) Immunofluorescence staining of neurons (green). Nuclei were stained with DAPI (blue). Scale bar=20µm. Results are

representative of two independent experiments performed in triplicate. Statistical analyses were performed with Graphpad Prism V6.0.1 using a two-tailed unpaired t test, **=p<0.01.

Figure 9 – Proposed model of interactions between TBEV and human brain cells

In the human brain parenchyma, TBEV infects neurons, astrocytes and possibly oligodendrocytes (1). Both neurons and astrocytes develop an antiviral response. In neurons, it is insufficient to afford protection (2) and poorly controlled infection induces neuronal death in a direct manner (3). Astrocytes are infected but control infection, owing to their strong antiviral response (4), which may also be beneficial to neurons (5). Astrocytes enter a reactive stage (6) and some of them die (7). Both neurons and astrocytes overexpressed a high level of chemokines involved in chemo-attraction of T cells in the brain parenchyma (8), although astrocytes are stronger producers. Figure was created using Servier Medical Art available on www.servier.com. As, astrocytes. AV Resp, antiviral response. CMK, Chemiokines. Ne, neurons.

Table 1 – Differential expression of genes involved in the human antiviral response in unsorted cultures (Uns-C), enriched neurons (En-N) and enriched astrocytes (En-As). Up and down-regulated genes appear in bold, after application of a cut-off of 3.

Supporting information legends

S1 Fig. Neurons and astrocytes are the major cell types in hNPCs-derived cultures.

940 HNPCs were differentiated for 13 days. (A) Immunofluorescence labeling using antibodies
941 against HuC/HuD, a neuronal nuclear marker (green), GFAP, an astrocytic marker (red) and
942 OLIG2, an oligodendrocyte nuclear marker (grey) were used. Nuclei were stained with DAPI
943 (blue). Scale bar=20 µm. (B) Enumeration of cells based on immunofluorescence labeling.
944 Automated quantification using an ArrayScan Cellomics instrument. (C) Enumeration of
945 astrocytes based on immunofluorescence labeling. Manual quantification.

946

947 **S2 Fig. – Neuronal survival is not affected by TBEV infection at 24 hpi in unsorted cells**
948 **and enriched neuron cultures.**

949 Unsorted cultures (Uns-C) and enriched neurons (En-N) were infected with TBEV and co-
950 immunostained with βIII-tubulin (neurons) and anti-TBEV-E3 antibodies. Manual enumeration
951 of infected neurons was performed at 24hpi. Data are expressed as the mean±SD and
952 normalized to non-infected Uns-C. Results are representative of two independent experiments
953 performed in triplicate. Statistical analysis was performed using a two-tailed unpaired t test with
954 GraphPad Prism V6.0.1, ns=non-significant ($p>0.05$).

955

956 **S1 Table -** Primer pairs used for qRT-PCR analyses.

957

959 **Supplementary Table 1. Primer pairs used for qRT-PCR analyses**

Gene name	3' primer	5' primer
GAPDH	CACCATCTTCCAGGAGCGAG	GAGATGATGACCCTTTTGGC
HPRT1	GGACTAATTATGGACAGGACTG	GCTCTTCAGTCTGATAAAATCTAC
TBEV	GGGCGGTTCTTGTTCTCC	ACACATCACCTCCTTGTCAGACT
TLR3	GCTGCAGTCAGCAACTTCAT	AGGAAAGGCTAGCAGTCATCC
DDX58 (RIG-I)	GAGAAAAAGTGTGGCAGCCT	ATATCCGGAAGACCCTGGAC
IFIH1 (MDA5)	TGCCCATGTTGCTGTTATGT	GTCTGGGGCATGGAGAATAA
CXCL10	GCAGGTACAGCGTACGGTTC	CAGCAGAGGAACCTCCAGTC
CXCL11	ATGCAAAGACAGCGTCCTCT	CAAACATGAGTGTGAAGGGC
CCL5 (RANTES)	TGTACTCCCGAACCCATTTC	TACACCAGTGGCAAGTGCTC
RSAD2 (viperin)	GTCCCTGGCATACAGAGACTG	GCTCAGAGGTTGCCTGAACA
IFI6	TCGCTGATGAGCTGGTCTGC	ATTACCTATGACGACGCTGC
OAS2	TGTTTTCCGTCCATAGGAGC	CTGATCGACGAGATGGTGAA
MX1	CTACACACCGTGACGGATATG	CGAGCTGGATTGGAAAGCCC
ISG15	CACCGTGTTCATGAATCTGC	CTTTATTTCCGGCCCTTGAT

960

961

962

Fig.1

(A)

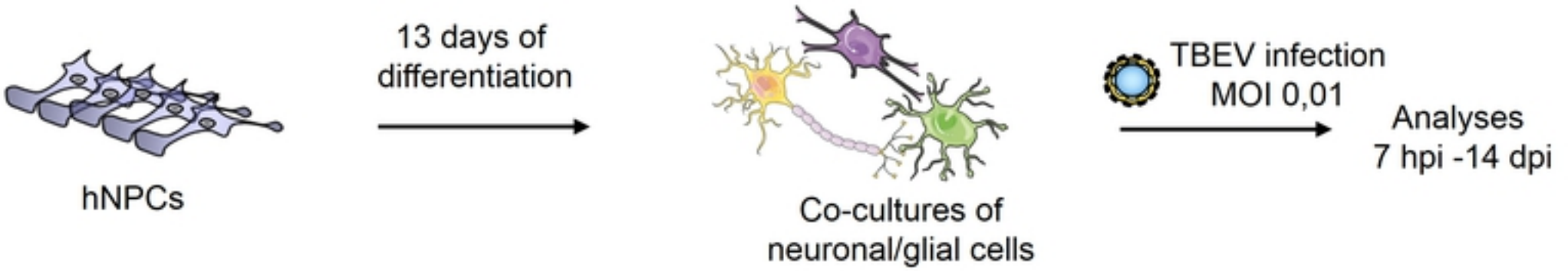

(B)

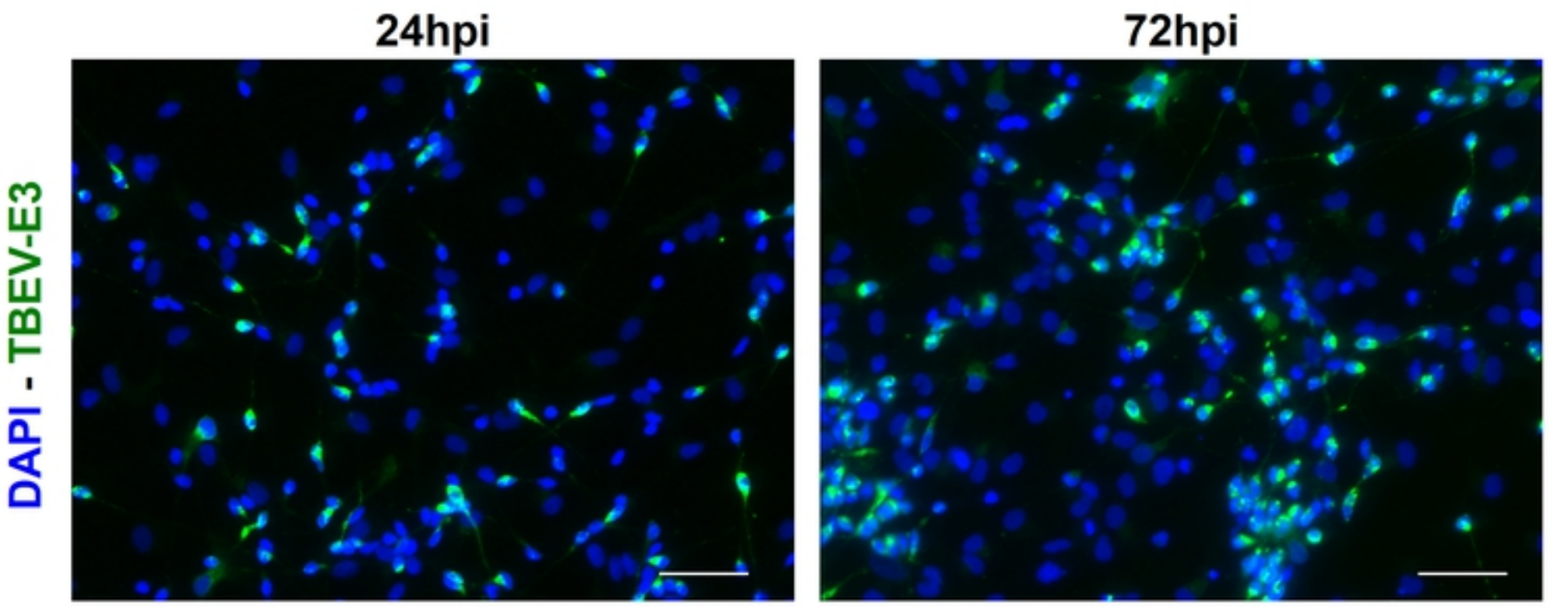

(C)

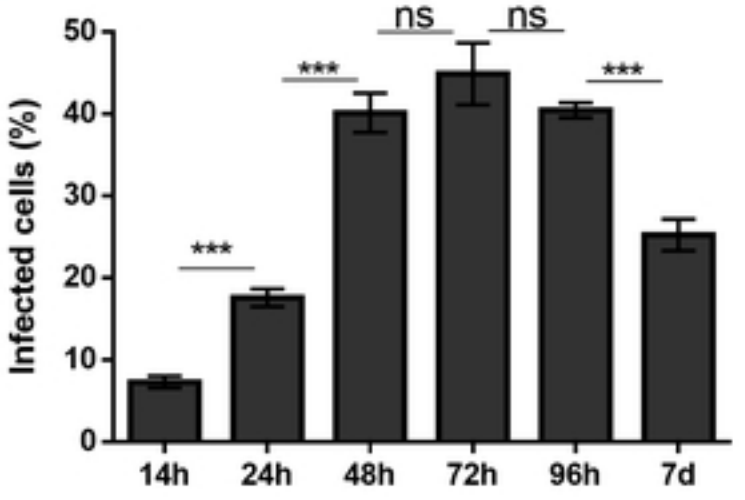

(D)

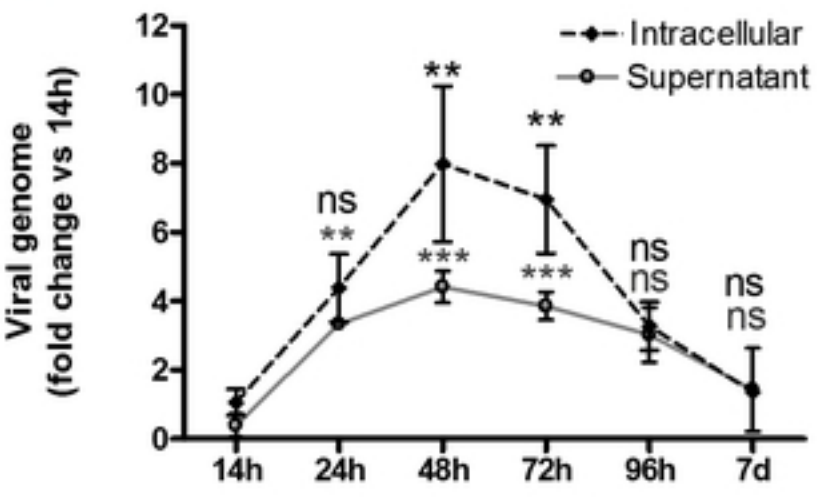

(E)

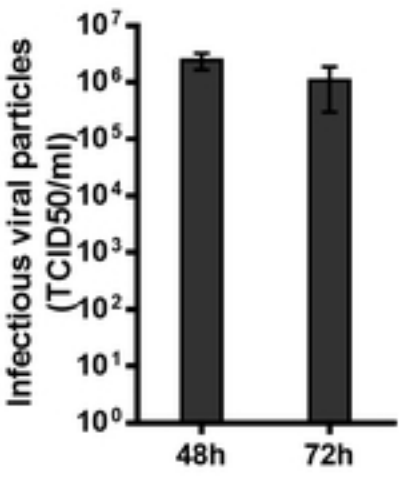

Figure 1

Fig.2

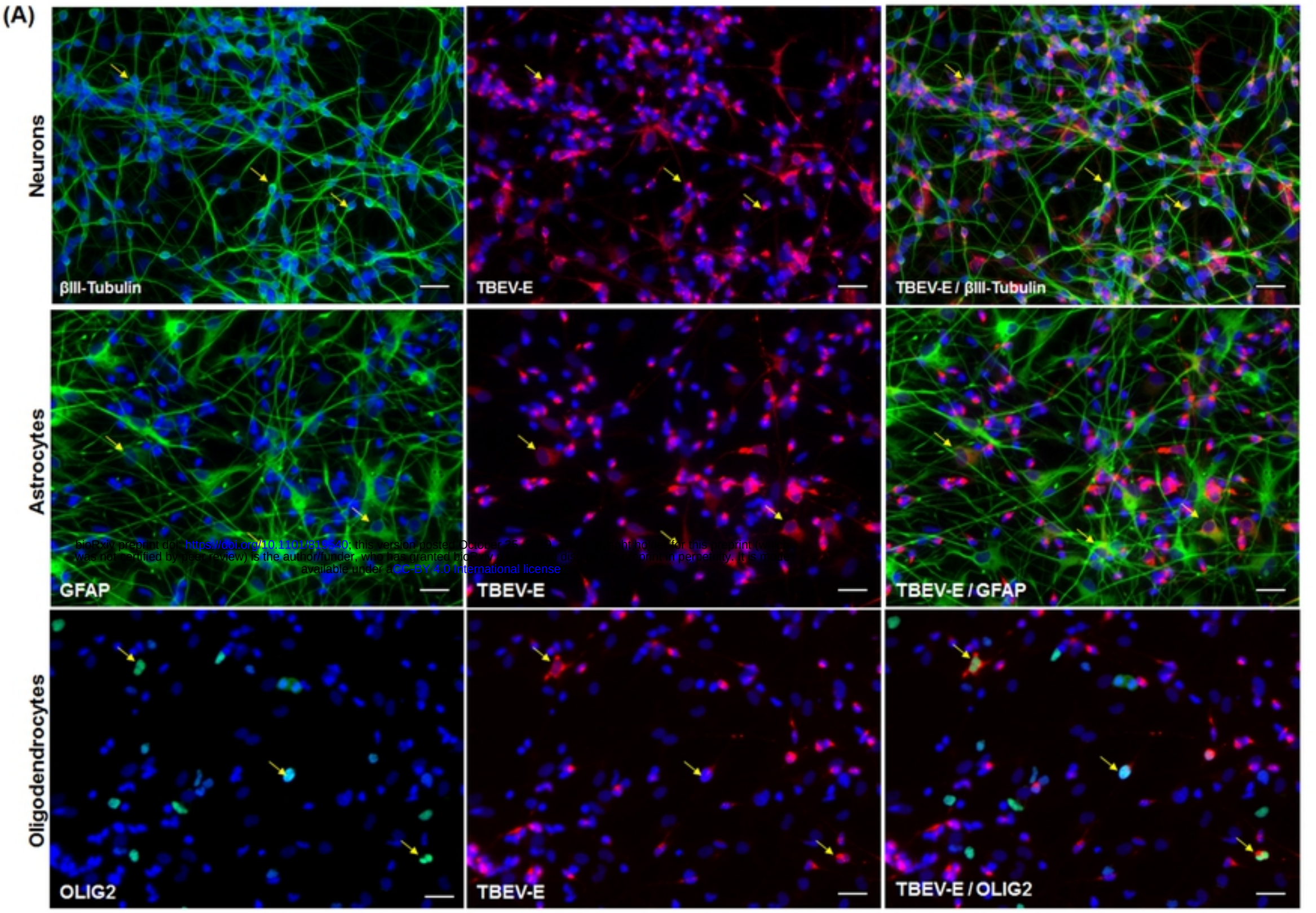

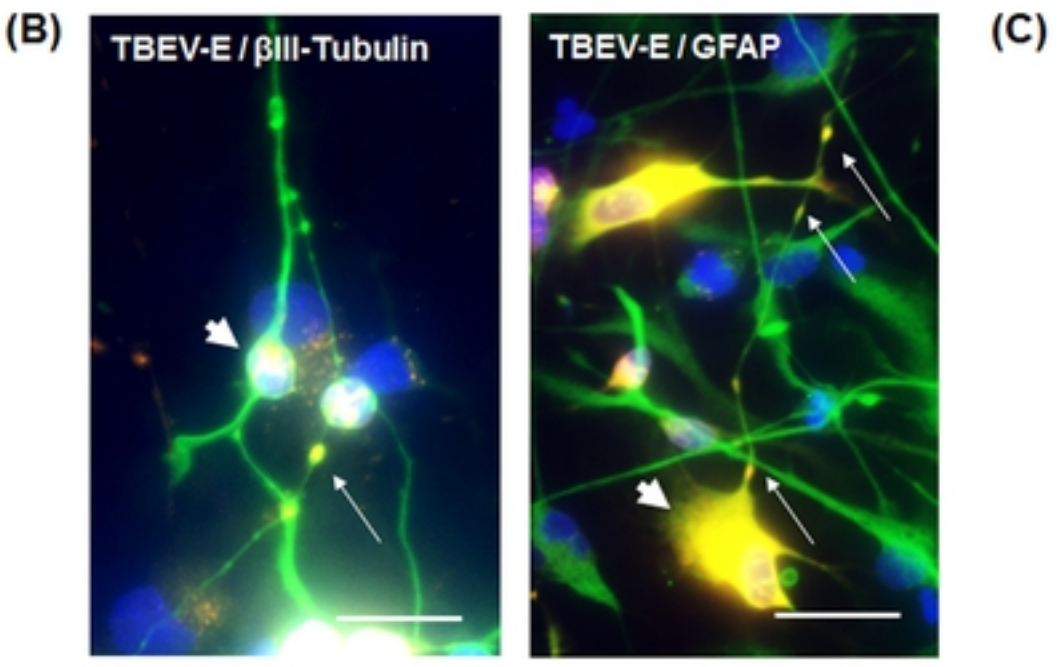

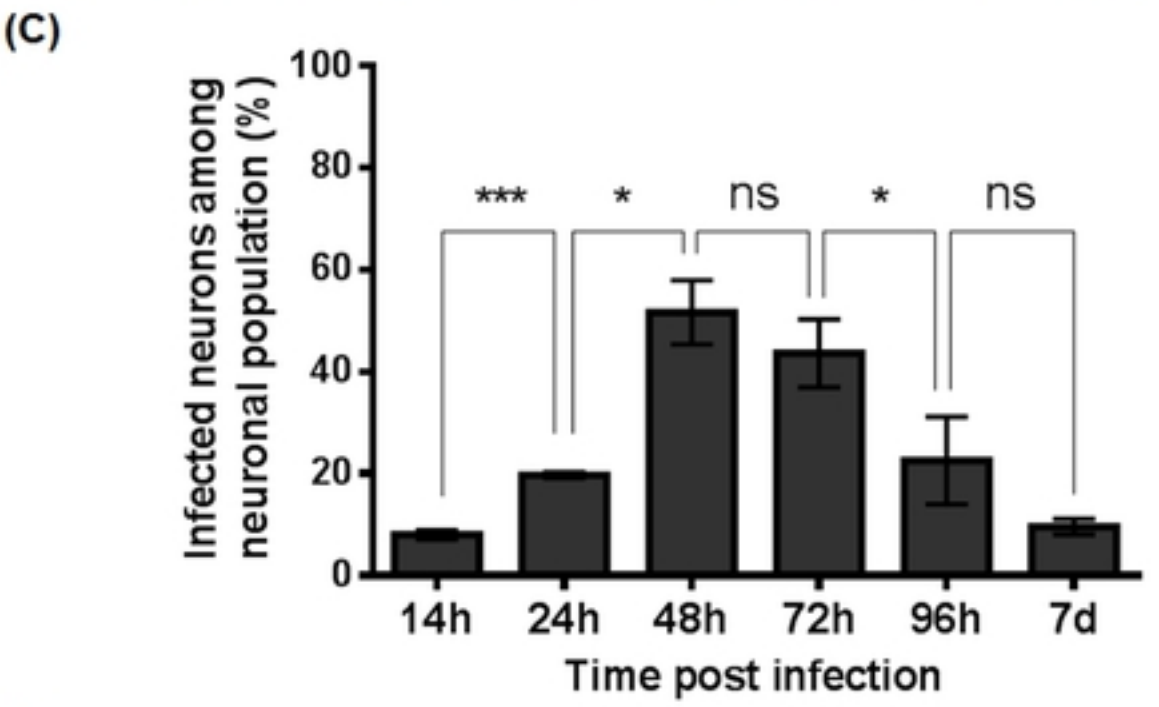

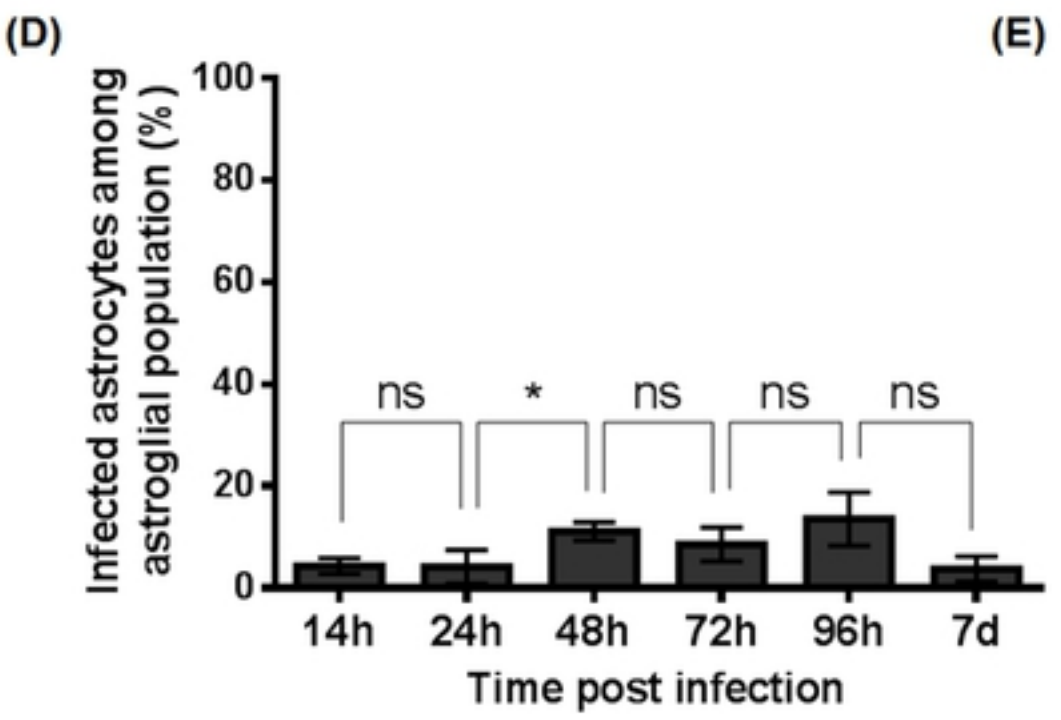

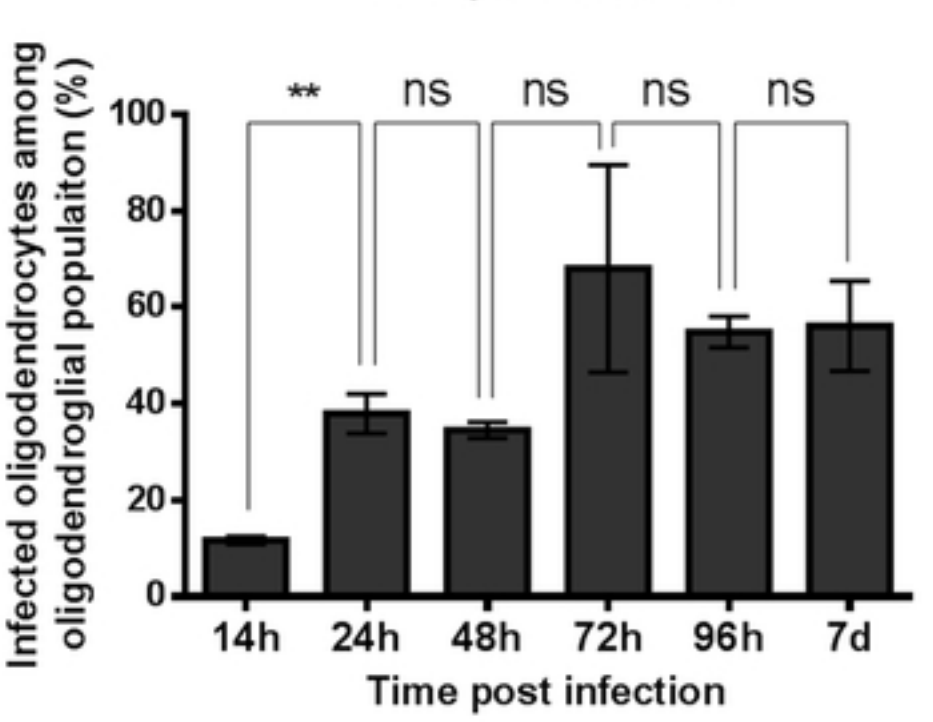

Figure 2

Fig.3

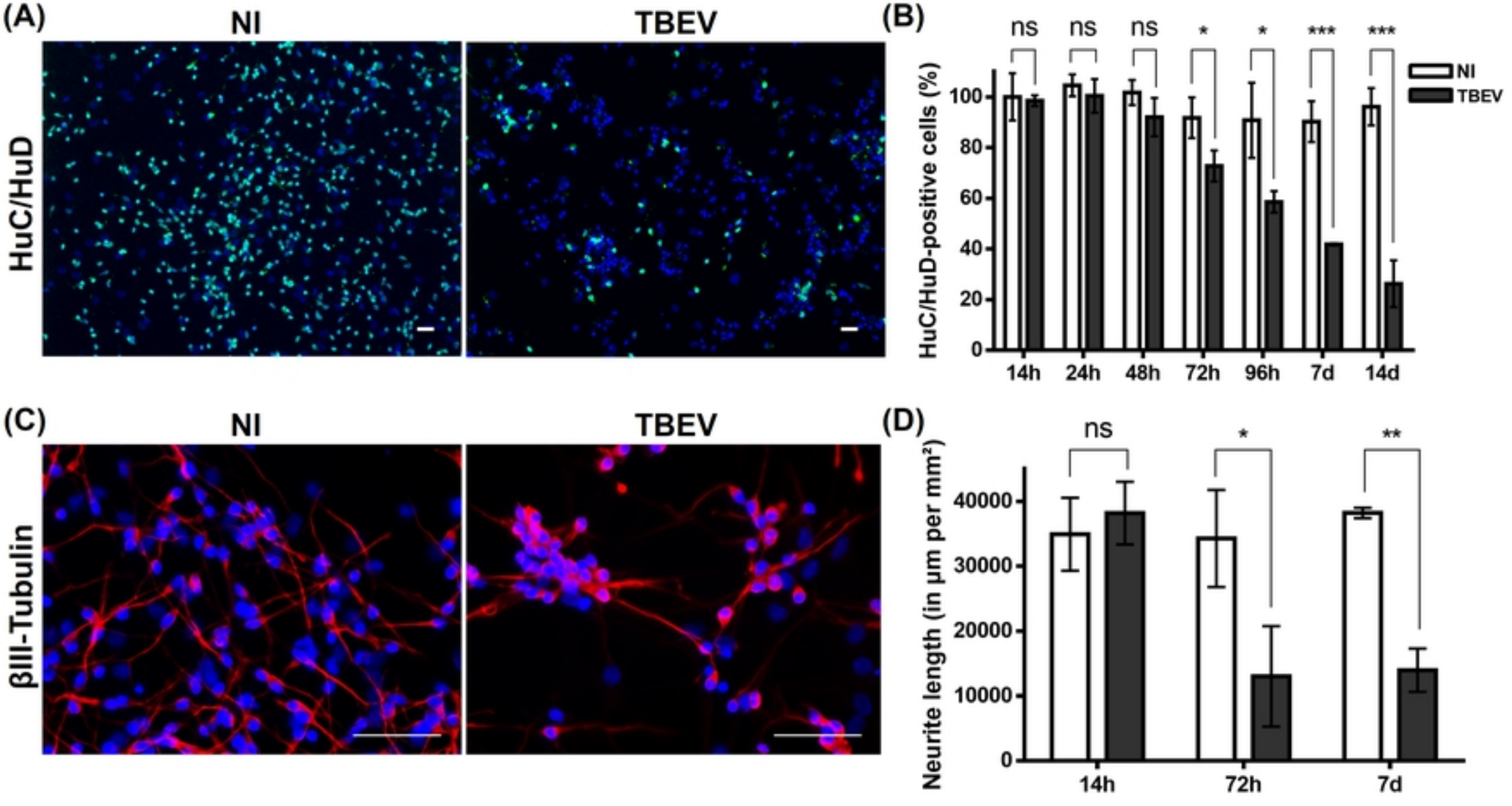

Figure 3

Fig.4

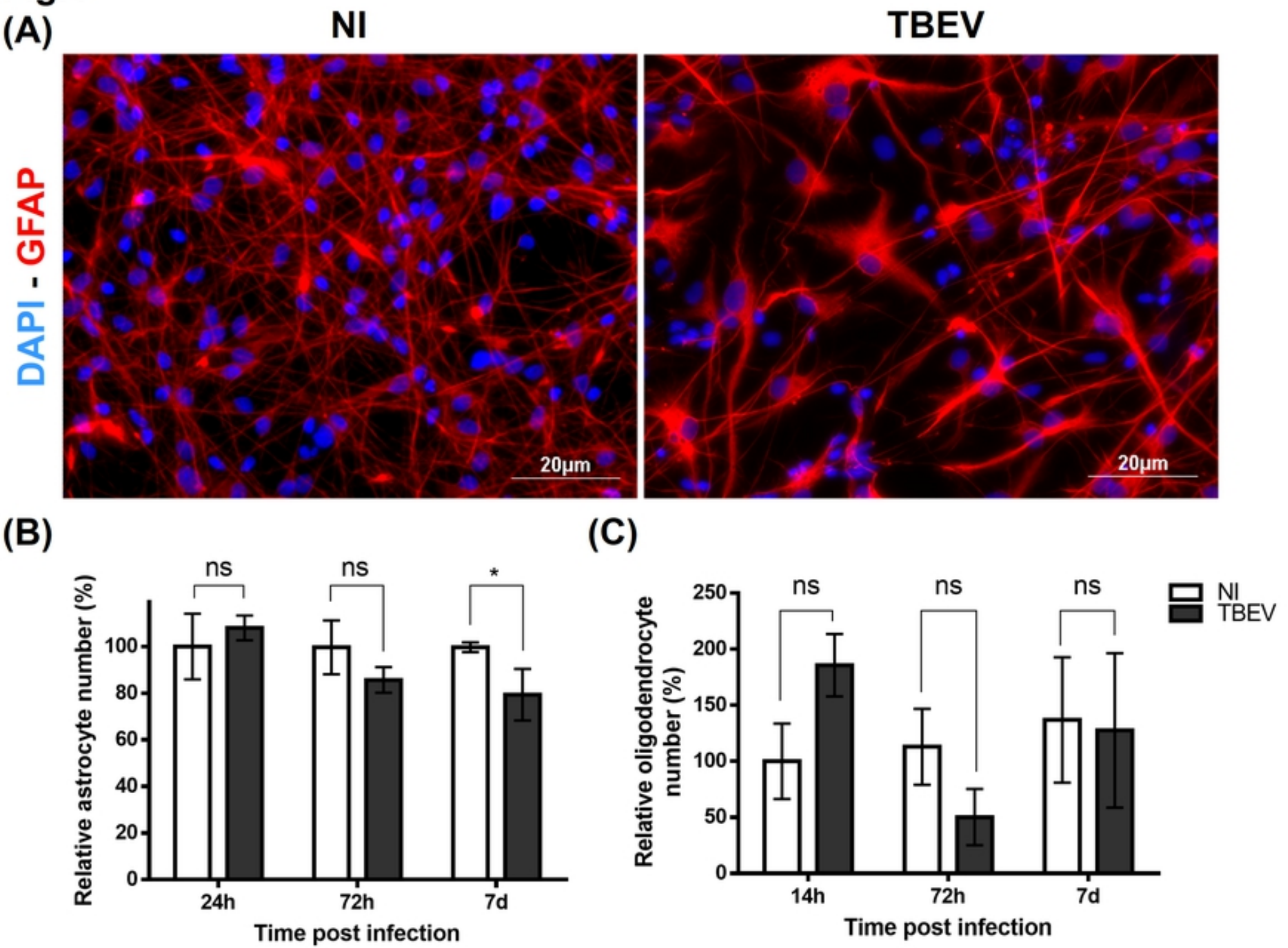

Figure 4

Fig.5

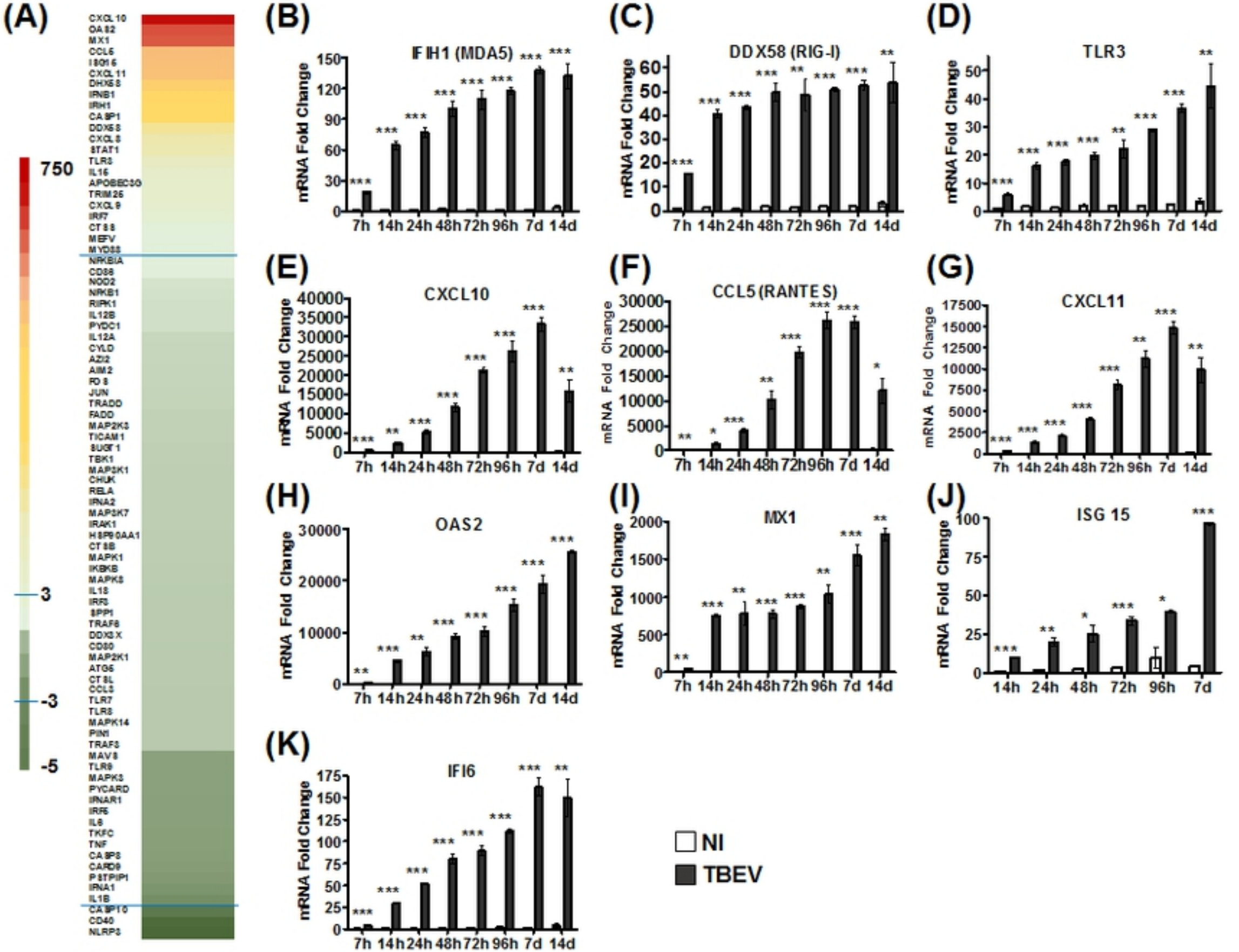

Figure 5

Fig.6

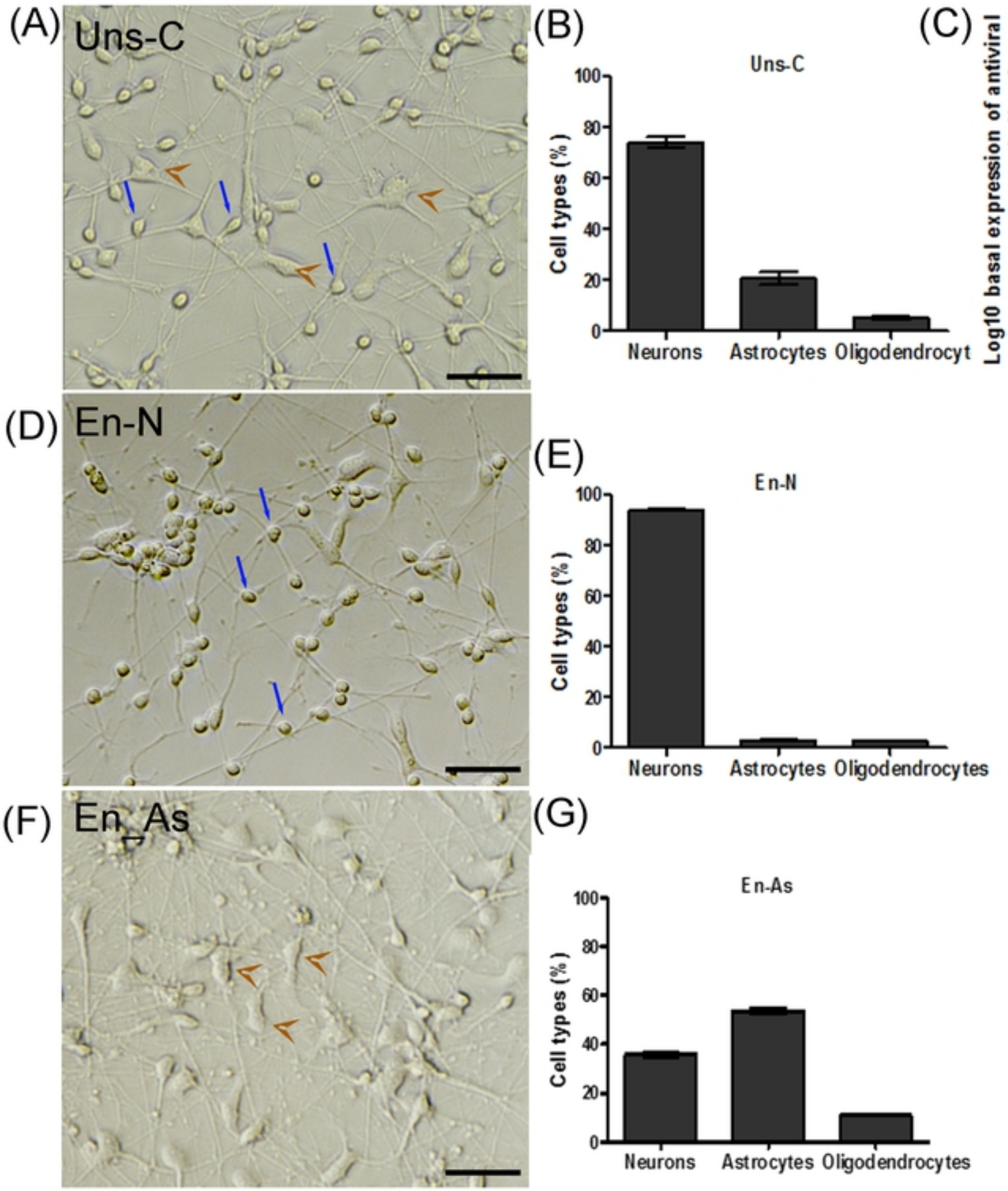

Figure 6

Fig.7

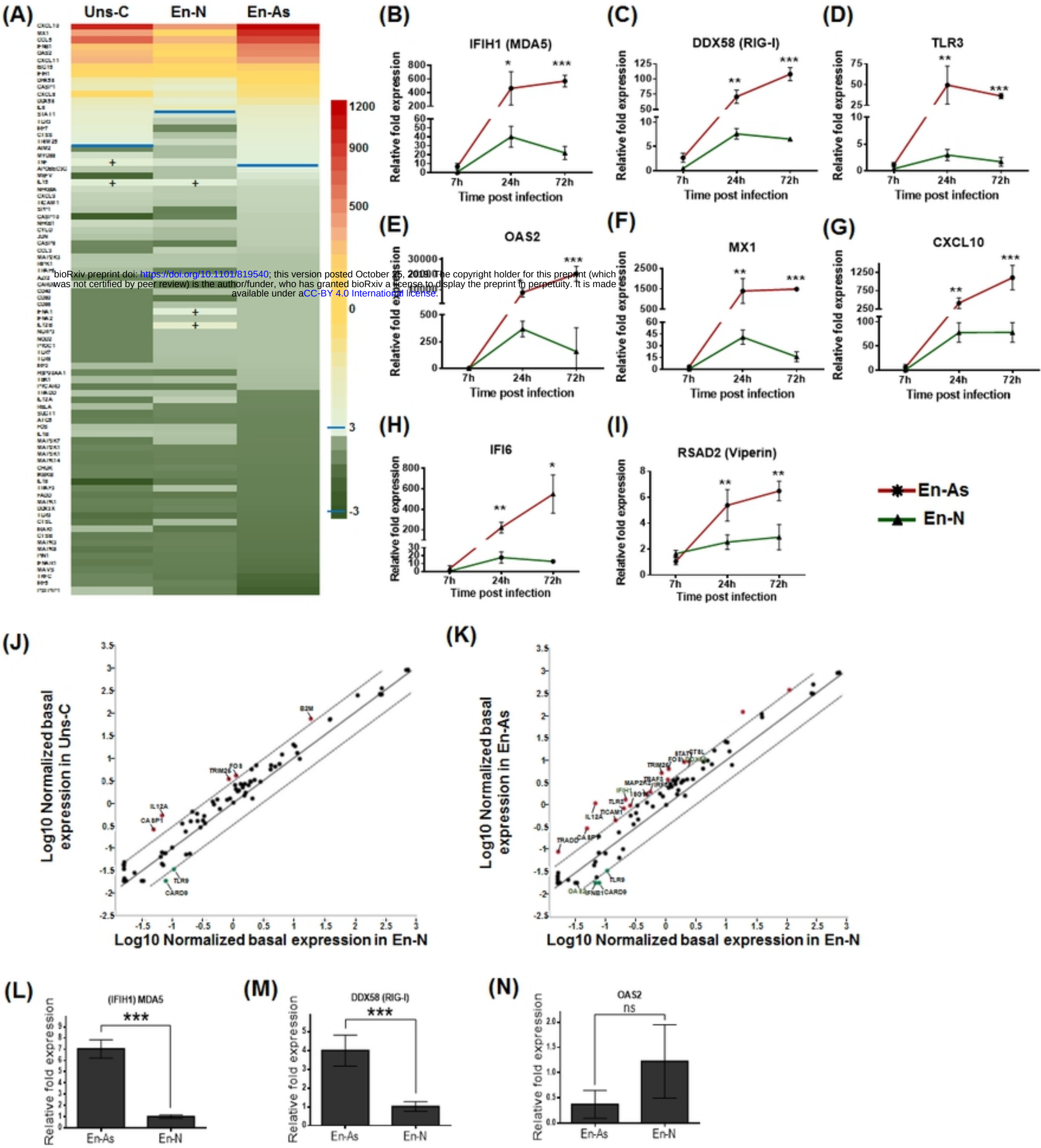

Figure 7

Fig.8

(A)

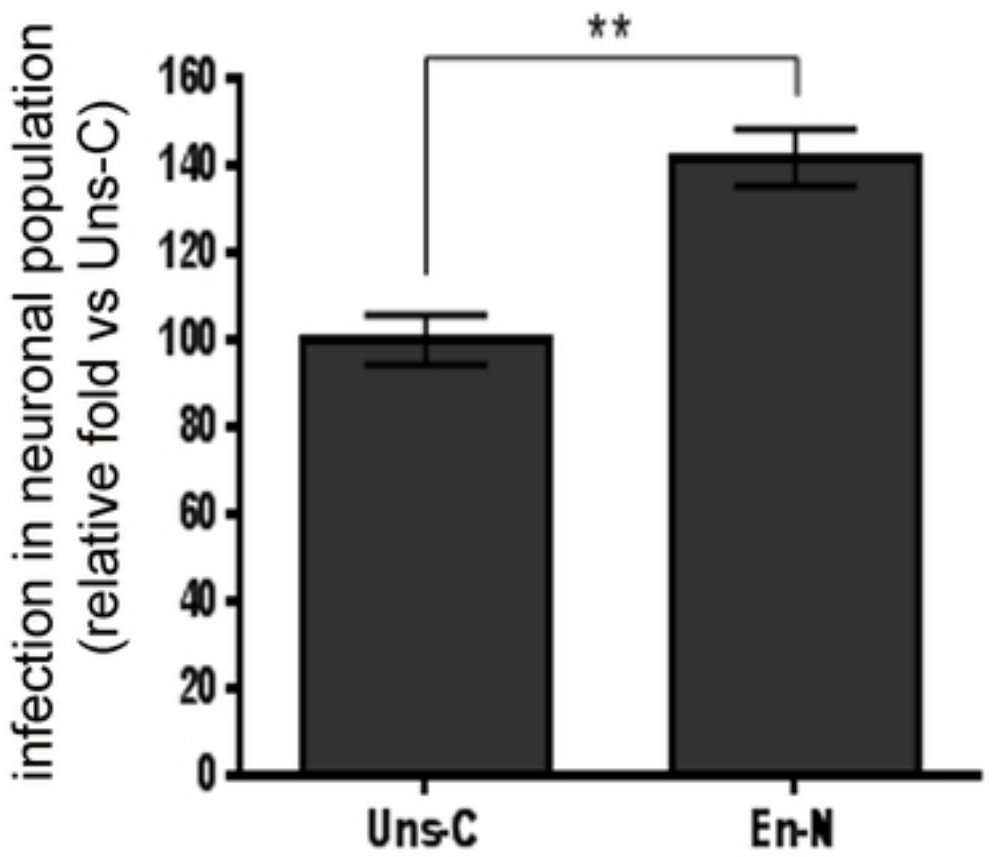

(B)

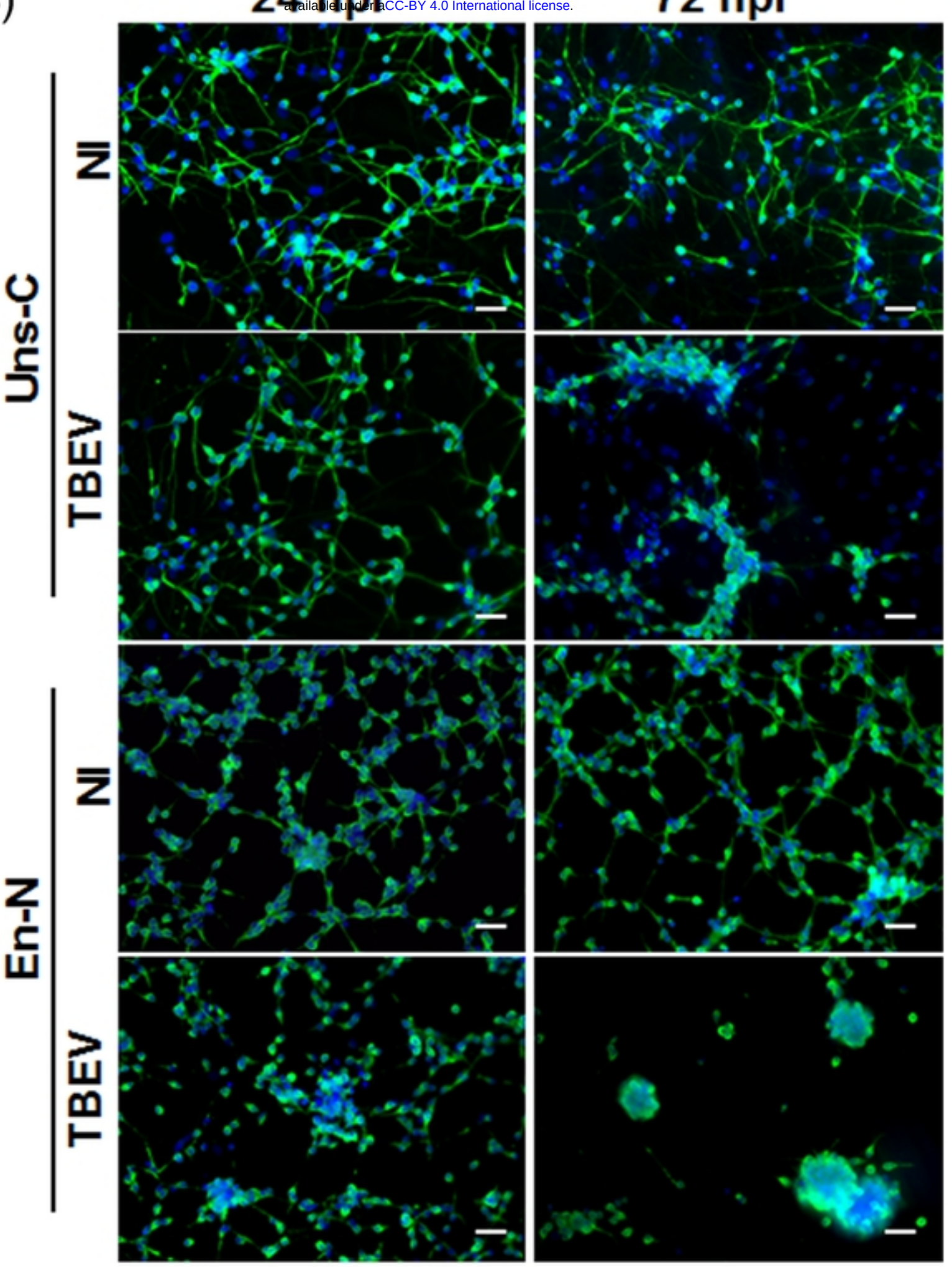

Figure 8

Fig.9

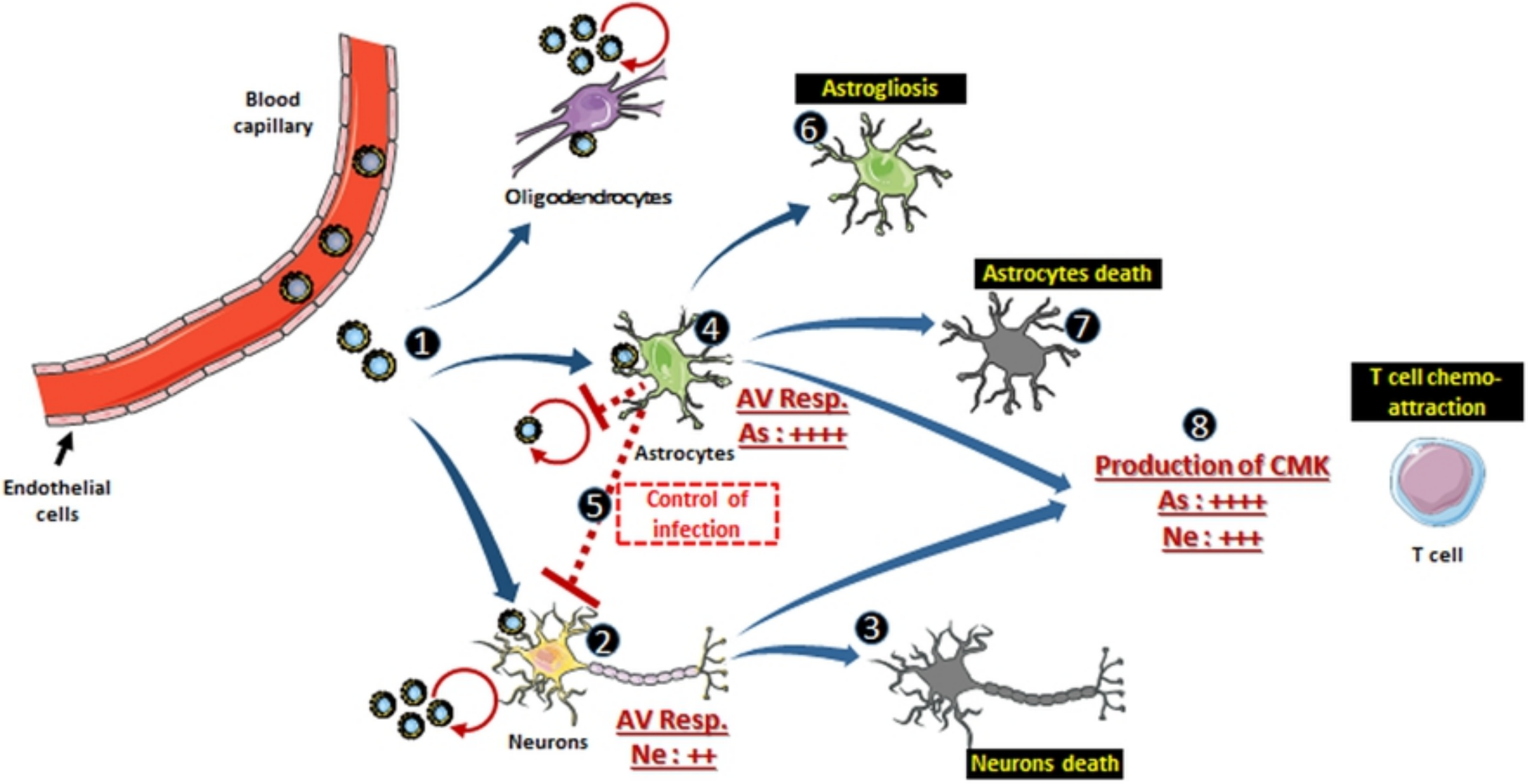

Figure 9

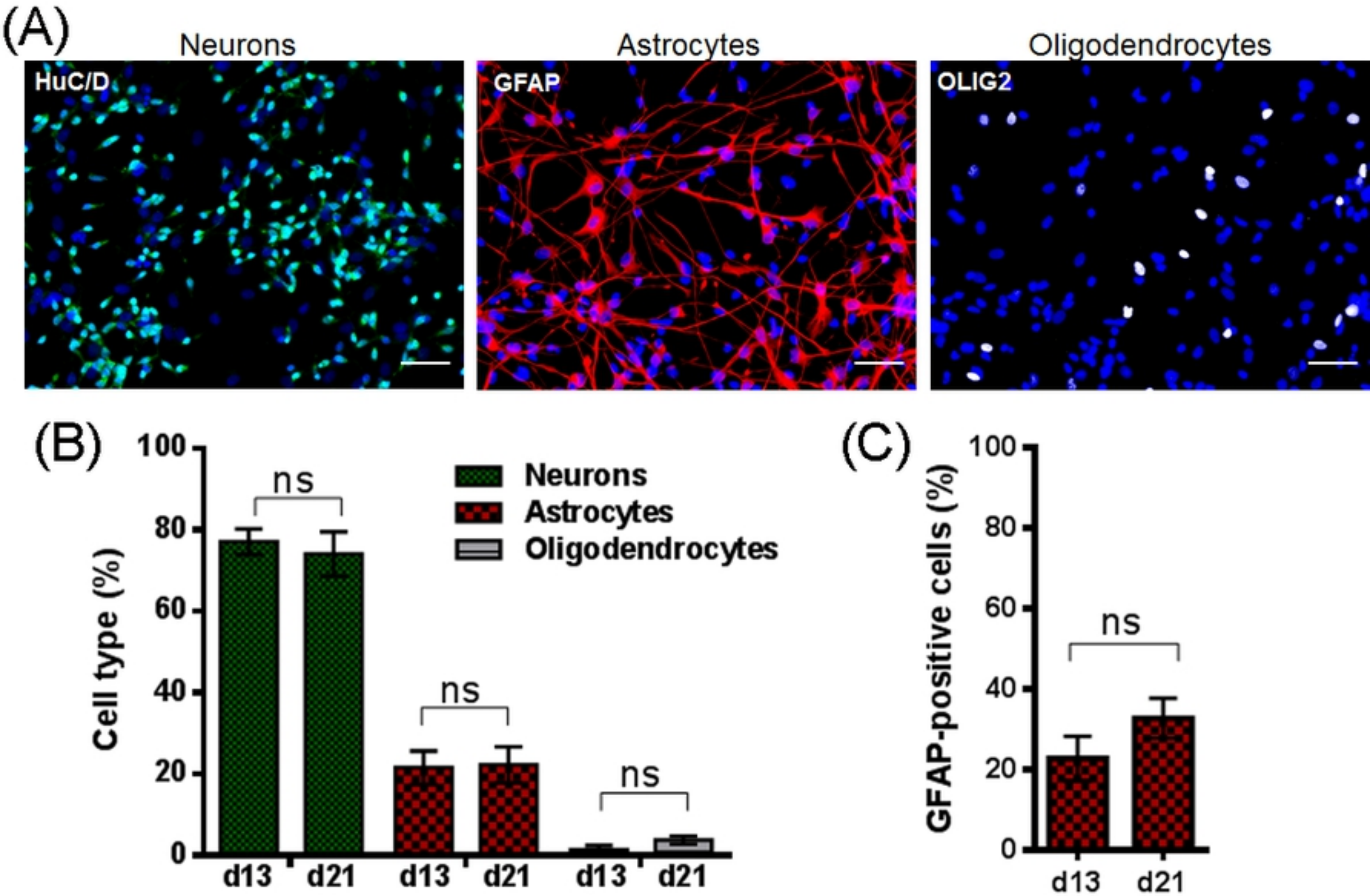
(A)
Neurons
Astrocytes
Oligodendrocytes
HuC/D
GFAP
OLIG2
(B)
Cell type (%)
100
80
60
40
20
0
ns
ns
ns
Neurons
Astrocytes
Oligodendrocytes
d13
d21
d13
d21
d13
d21
(C)
GFAP-positive cells (%)
100
80
60
40
20
0
ns
d13
d21

S2 Fig

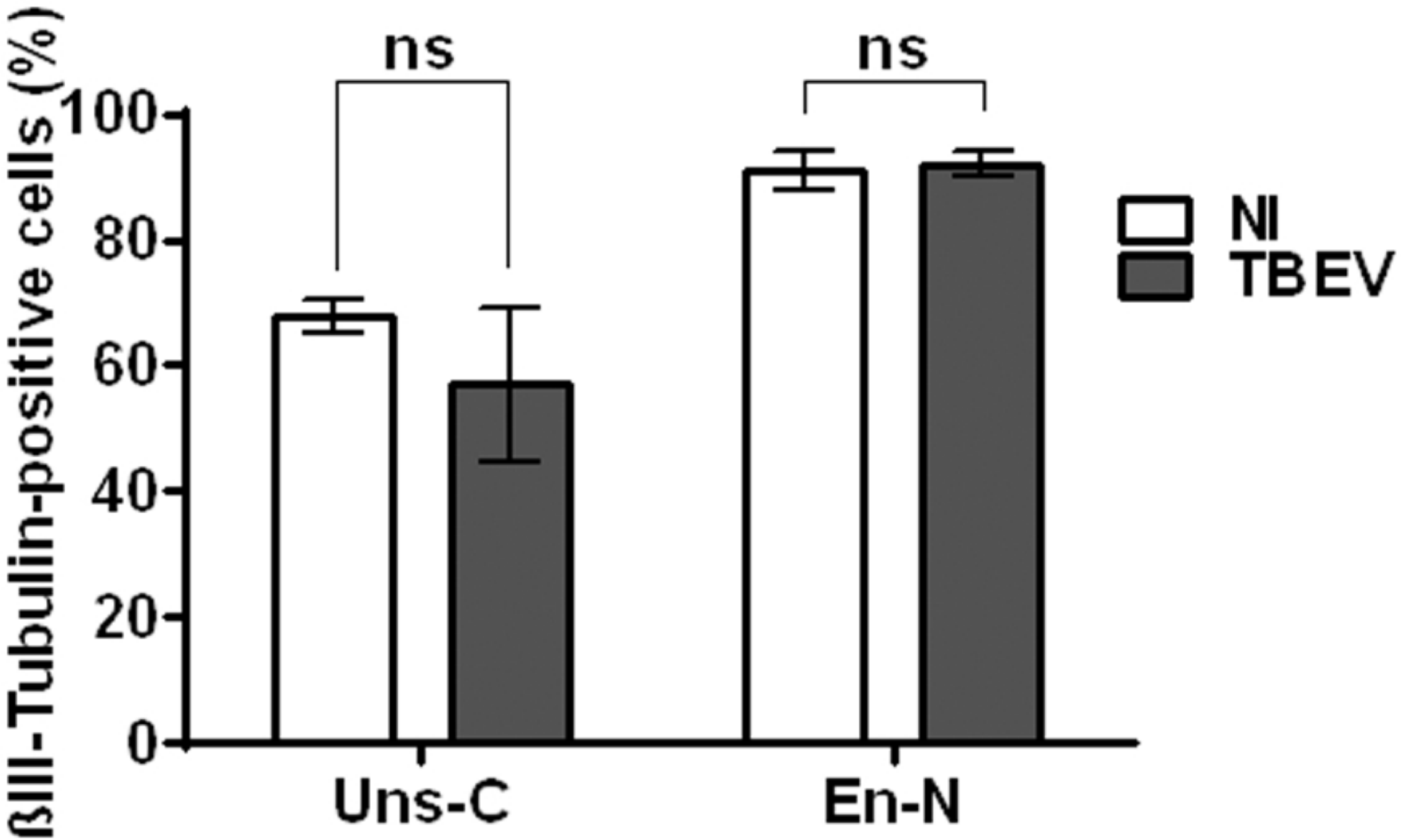

S2 Fig